OBSERVING SUPPRESSION OF MICROBIAL GROWTH WITH SURFACE-ENHANCED RAMAN SCATTERING

by
Melike Belenli

Submitted to Graduate School of Natural and Applied Sciences
in Partial Fulfillment of the Requirements
for the Degree of Master of Science in
Biotechnology

Yeditepe University
2019

OBSERVING SUPPRESSION OF MICROBIAL GROWTH WITH SURFACE-ENHANCED RAMAN SCATTERING

APPROVED BY:

Prof. Dr. Mustafa Çulha .....
(Thesis Supervisor)
(Yeditepe University)

Prof. Dr. Hatice Gülen .....
(İstanbul Bilgi University)

Assist. Prof. Dr. Andrew Harvey .....
(Yeditepe University)

DATE OF APPROVAL: ..../..../2019

ACKNOWLEDGEMENTS

It is with immense gratitude that I acknowledge the support and help of my Professor Mustafa Çulha. I am thankful to him for his directive comments, suggestions, guidance and patience during my thesis period.

Also, I would like to thank my Head of Department at Istanbul Bilgi University, Professor Hatice Gülen, for encouraging me not to give up and being sympathetic throughout my thesis study.

I am also thankful to my friends Dr. Özlem Şen and Dr. Melis Emanet who were the best part of this longer-than-expected master study. I know that without their guidance, support, solidarity, but most importantly without their friendship, it would be nearly impossible to finish this study.

Also, I want to thank all the people in the Nanobiotechnology Group for always being there when I need something. A special thanks to Dr. Seda Keleştemur for her valuable advices, it was good to know having someone who can help you with her knowledge even after her graduation. I also thank Dr. Hülya Yılmaz, Hande Duru, Zehra Çobandede, Deniz Uzunoğlu, Melike Sarıçam, Ayşe Çınkılıç, Şaban Kalay and Sadık Kalaycı for their help and supports.

Special thanks to my heroes on the other side of the city, Semra Özdemir Salihoğlu and Tuğba Köse, for being there with all of their knowledge, sympathy and support whenever I need. I would like to thank Dr. Çiğdem Sezer Zhmurov and Dr. Müge Kesici for sharing their invaluable experiences especially about academic life. I also want to thank my colleagues at Istanbul Bilgi University Ergin Kükrer, Perihan Ünver Uçkaç, Canberk Yıldırım and Serkan Karatosun who are not just my colleagues but my friends.

My family, both the nucleus and the big one, deserves the greatest thanks for being warm-hearted, supportive, but most importantly endlessly patient during almost six years. I would like to thank my father, Tahir Belenli, who spent lots of nights in the lab with me, and my mother, İzdihar Belenli, who felt exactly the same stress and anxiety as I was feeling during this period. I am glad to free all of us from this burden. Also thank you my

brother, Niyazi Enes Belenli, I know that you are there for me when I am down. I also thank my beloved grandmother, Tefrize Belenli, for being an inspiration for me. Then, I would like to thank my new family, Nurhan Gümüş, Muhsin Gümüş and Selenay Gümüş for their care, love, support and patience. It was a pleasure to give some good news to you.

I cannot pass without mentioning my girl powers; my precious Şükriye Türkoğlu, my sisters Ayşen İpek and Gülşen Çakmak, and my dear friends Meryem Şahin and Vildan Bayram. Whenever I felt hopeless, you were there for me, thank you.

Last but not least, my deepest gratitude is to my beloved boyfriend, Gökhan Gümüş, who is my source of motivation not just for graduation but for life. I would have already given up and lost without your love, encouragement, and support. Thank you for believing in me while even I did not believe in myself. Thank you for all of your efforts for me; I cannot imagine a better companion to share the journey of life.

Finally, I would like to thank my lost ones; my grandfathers Hacı Mehmet Çakmak and Niyazi Belenli, and my grandmother Şerife Çakmak. If I can ever do something beautiful, it will be because of you. Your love and kindness will never be forgotten. Thank you.

ABSTRACT

OBSERVING SUPPRESSION OF MICROBIAL GROWTH WITH SURFACE-ENHANCED RAMAN SCATTERING

Microorganisms can be both harmful and beneficial for human depending on their nature. If the mechanisms that make them harmful are known, their detrimental effects can be minimized, which makes the study of microbial growth crucial. The amount of nutrients plays an important role on the growth as well as presence of different chemicals that are toxic to them. Observation of microbial growth in different environmental conditions is important in terms of understanding the growth mechanisms of microorganisms. Among many analytical and spectroscopic methods, Surface-Enhanced Raman Scattering (SERS) is a promising technique to work with biological samples. It gives valuable information about molecular structures based on their vibrational modes. While working with biological samples, it has many advantages such as simple sample preparation, no interference from water and achieving low limits of detection.

In the thesis presented below, microbial growth of bacteria and yeast cells in the presence of a biocidal agent were investigated with SERS. Maltose-reduced silver nanoparticles (m-AgNPs) were used as biocidal agent. *Escherichia coli* (*E.coli*) and *Saccharomyces cerevisiae* (*S.cerevisiae*) were selected as model organisms for bacteria and yeast, respectively. The effect of three different concentrations (5, 10, and 20 ppm) of m-AgNPs were tested on the mentioned microorganisms. Their microbial growth was monitored by both measuring optical density (OD) and collecting their Raman scattering under a laser beam. The spectral changes with respect to time were analyzed and the bands related to certain metabolites of microorganisms such as amino acids, carbohydrates, proteins and genetic material were used to monitor the changes in the chemical composition of cell cultures. Results of both analysis revealed that microbial growth of *E.coli* is suppressed when the cells are treated with 5 and 10 ppm m-AgNPs, and is inhibited in the presence of 20 ppm m-AgNPs. The results obtained from *S.cerevisiae* demonstrates suppression of its growth increses with the increasing concentration of m-AgNPs as well.

ÖZET

MİKROBİYAL BÜYÜMENİN BASKILANMASININ YÜZEYDE ZENGİNLEŞTİRİLMİŞ RAMAN SAÇILMASI İLE GÖZLEMLENMESİ

Mikroorganizmalar doğalarına bağlı olarak insanlar için faydalı veya zararlı olabilirler. Zararlı olmalarına neden olan mekanizmaları bilmek, bu etkileri en az düzeye indirmeyi sağlayabilir. Mikroorganizmaların çevresinde bulunan besin maddelerinin mikarı kadar etraflarında bulunabilecek zehirli kimyasalların da büyümeleri üzerinde önemli etkisi vardır. Mikrobiyal büyümenin farklı çevresel koşullarda incelenmesi, mikroorganizmaların büyüme mekanizmalarının anlaşılması açısından önemlidir. Bir çok analitik ve spektroskopik metod arasından yüzeyde zenginleştirilmiş Raman saçılması (YZRS) biyolojik örneklerle çalışmak için umut vaat eden bir tekniktir. YZRS moleküllerin titreşim modlarına bağlı olarak molekül yapıları ile ilgili önemli bilgiler sağlar. YZRS için örnek hazırlamanın kolay olması, alınan spektrumun sudan etkilenmemesi ve az miktarda örneğin yeterli olması, YZRS'nin biyolojik örneklerin analizinde kullanılmasını avantajlı hale getirir.

Bu tezde, bir biyosidal ajanın bakteri ve maya hücrelerinin büyümesine etkisi YZRS ile incelenmiştir. Biyosidal ajan olarak, maltozla-indirgenmiş gümüş nanoparçacıklar kullanılmıştır. Bakteri hücresine model olarak *Escherichia coli* (*E.coli*), maya hücresine model olarak ise *Saccharomyces cerevisiae* (*S.cerevisiae*) seçilmiştir. Gümüş nanoparçacıkların bahsedilen mikroorganizmalar üzerindeki etkisi üç farklı konsantrasyonda (5, 10, ve 20 ppm) incelenmiştir. Mikrobiyal büyümeleri hem optik yoğunlukları ölçülerek hem de lazer ışını altındaki Raman saçılmaları toplanarak izlenmiştir. Zamana bağlı olarak gözlenen spektral değişiklikler analiz edilmiş ve amino asitler, karbonhidratlar, proteinler ve genetik materyalden gelen pikler kullanılarak hücre kültüründeki kimyasal maddelerin içeriğindeki değişimler izlenmiştir. Yapılan iki analizin ışığında, 5 ve 10 ppm gümüş nanoparçaçıkla inkübasyonun *E.coli*'nin büyümesini baskıladığı, 20 ppm konsantrasyonda ise büyümenin hiç gözlemlenmediği anlaşılmıştır. *S.cerevisiae*' den alınan sonuçlarda ise büyümenin baskılanmasının artan gümüş nanoparçaçık konsantrasyonu ile doğru orantılı olarak arttığı gözlemlenmiştir.

TABLE OF CONTENTS

LIST OF FIGURES

LIST OF TABLES

LIST OF SYMBOLS/ABBREVIATIONS

µl	Microliter
°C	Degrees Celsius
g	Gram
h	Hour
mL	Milliliter
nm	Nanometer
ppm	Parts per million
Ag	Silver
Ag^+	Silver ions
$AgNO_3$	Silver nitrate
AgNPs	Silver nanoparticles
ATP	Adenosine triphosphate
Au	Gold
AuNPs	Gold nanoaprticles
C	Carbon
c-AgNPs	Citrate-reduced silver nanoparticles
C. albicans	*Candida albicans*
CaF_2	Calcium fluoride
CuO	Copper(II) oxide
ddH_2O	Double-distilled water
DLS	Dynamic light scattering
DNA	Deoxyribonucleic acid
E. coli	*Escherichia coli*
FAD	Flavin adenine dinucleotide
IR	Infrared
LB	Lysogeny broth
LOD	Limit of detection
LSPR	Localized surface plasmon

m-AgNPs	Maltose-reduced silver nanoparticles
MIC	Minimum inhibition concentration
N	Nitrogen
NiO	Nickel(II) oxide
O_2	Oxygene
OD	Optical density
POC	Point-of-care
PVP	Polyvinylpyrrolidone
RNA	Ribonucleic acid
ROS	Reactive oxygen species
S	Sulphur
Sb_2O_3	Antimony oxide
SDB	Sabouraud dextrose broth
SERS	Surface-enhanced Raman scattering
SP	Surface plasmon
SPP	Surface plasmon polarition
SPR	Surface plasmon resonance
UV-Vis	Ultraviolet-Visible
ZnO	Zinc oxide

1. INTRODUCTION

1.1. AIM OF THE STUDY

Aim of this study is to monitor the effect of maltose-reduced AgNPs (m-AgNPs) on microbial growth of different microorganisms such as bacteria and yeast by using Surface-Enhanced Raman Spectroscopy (SERS).

For this purpose, *Escherichia coli (E.coli)* cells were selected as model bacteria and *Saccharomyces cerevisiae (S.cerevisiae)* cells were selected as model yeast cells. Lysogeny Broth (LB) medium for *E.coli* and Sabouraud Dextrose Broth (SDB) for *S.cerevisiae* were used as growth media. In order to investigate how different concentrations of m-AgNPs affect the microbial growth of different microorganisms, LB and SDB media were mixed with different amounts of m-AgNPs. The cells were incubated with their media which contain different amounts of m-AgNPs. Samples were taken for SERS analysis at the end of certain incubation times. The spectra obtained from the samples were analysed and the changes in the metabolite profiles due to the presence of m-AgNPs in the media through the changes in spectral pattern band intensities were examined by comparing their spectra with the spectrum of control group, which does not contain any m-AgNPs.

1.2. MICROORGANISMS

Microorganism is a general name given to several different types of living organisms of microscopic size. These micron-size creatures are both beneficial and detrimental for humanity at the same time. As an example for the benefits of microorganisms, it can be said that the cycles of many elements such as carbon, nitrogen and phosphorus cannot be fulfilled without them. On the other hand, they are the main cause of many deadly diseases.

Microorganisms are mostly unicellular organisms which are capable of performing essential processes of life such as growth, metabolism and reproduction. They can be divided into two groups based on the differences in cellular organization and biochemistry.

Archaea, being the first domain of life, belong to prokaryotes along with one of the well-known microorganisms, bacteria. Other unicellular organisms such as fungi, protozoa and slime moulds form the group of eukaryotes [1]. The main difference between prokaryotic and eukaryotic cells is the latter have membrane-enclosed organelles. Prokaryotic cells do not have separate organelles; they consist of a cell wall, cell membrane, cytoplasm, nucleoid, ribosome and plasmid. As they do not have separate compartments like eukaryotic cells, all metabolic activity and protein synthesis take place in cytoplasm. Also they do not have a separated nucleus for their genetic material; their DNA is condensed in nucleoid. However, eukaryotic cells have more complex cellular structure than prokaryotes. They have membrane-bound organelles in their cytoplasm, and these organelles carry out different tasks for the survival of the cell. Unlike prokaryotes, eukaryotes have their DNA in nucleus, separated from cytoplasm by a double-membrane structure [2].

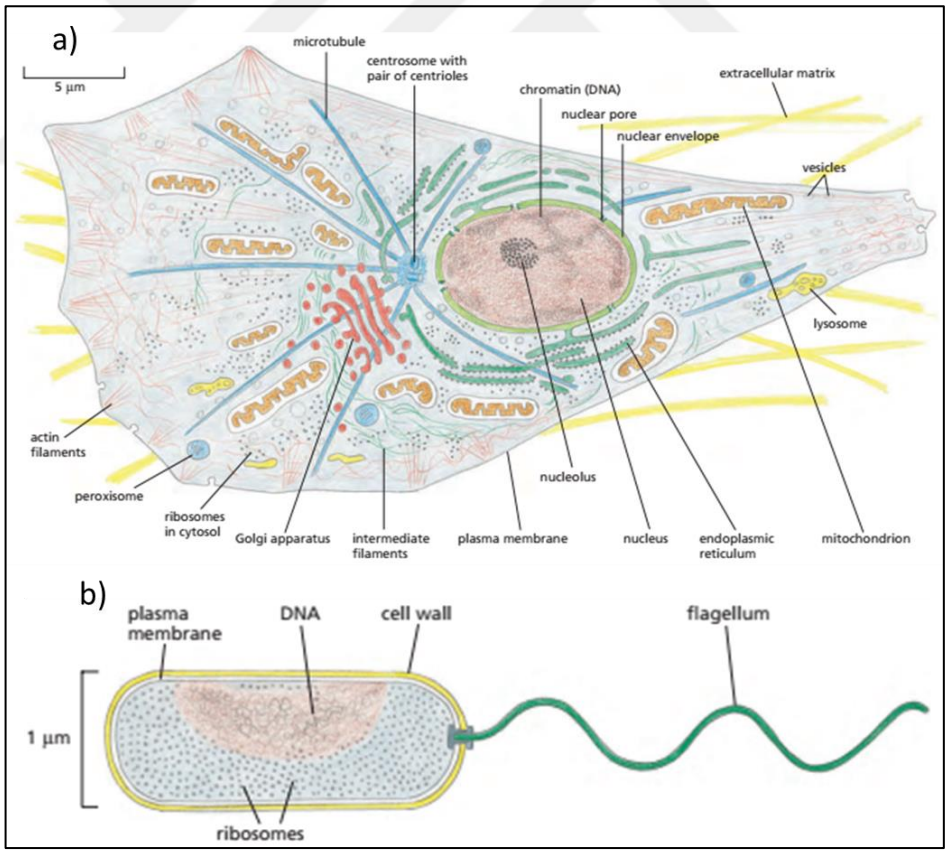

Figure 1.1. Representation of a) eukaryotic and b) prokaryotic cells with their cell components [3]

Bacteria comprise vast amount of prokaryotes, and they can be found everywhere in *biosphere*. They have the least complex cellular structure among microorganisms. They are very diverse and can be classified based on their differences in cell components, cell structure, or cellular metabolism. One of the famous classification methods is named as Gram-staining after the Danish bacteriologist Hans Christian Gram who developed the technique. This technique depends on the structural differences of bacterial cell wall. For most of the bacteria, cell wall is made of peptidoglycan layer which is a polymer consisting of sugars and amino acids. Depending on the thickness of peptidoglycan layer, cell wall can be stained purple by crystal violet or counter-stained pink by safranin. If bacterial cell wall is composed of a thick peptidoglycan layer, crystal violet become trapped within this structure and stained purple. This group of bacteria are called as Gram-positive bacteria. If bacterial cell wall is composed of a thinner peptidoglycan layer, it loses its purple colour after washing and can be stained pink by a counter-stain. In this case bacteria are called as Gram-negative as they are not stained with Gram stain [4,5].

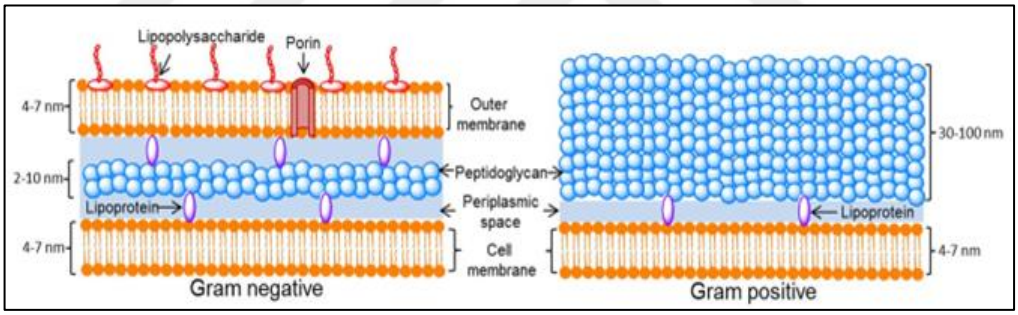

Figure 1.2. Schematic illustration of Gram-negative and Gram-positive bacteria [4]

Eukaryotic microorganisms such as fungi and parasites can be either unicellular or multicellular and have a much more complex cellular structure compared to bacteria. They have membrane-bound organelles that are responsible of specific functions of the cell. Some examples of organelles can be given as; mitochondria which is responsible for energy generation, endoplasmic reticulum produces and transports proteins and golgi body which delivers molecules throughout the cell and responsible for exocytosis and secretion [6]. Among eukaryotic microorganisms, kingdom of fungus includes yeasts and molds. Yeasts are unicellular fungi whereas molds grow in the form of multicellular filaments. They are both heterotrophs and responsible for decomposing in ecological systems. They have a cell wall which is composed of carbohydrates such as β(1,3) glucan and β(1,6)

glucan, mannoprotein and chitin. Although there are many yeasts related with infection and diseases such as *Candida albicans* [7], many forms of yeasts are used in fermentation processes in industry such as alcohol production, making bread and probiotics. Also, they can be used in bioremediation and they are very useful as model organisms in scientific researches [8].

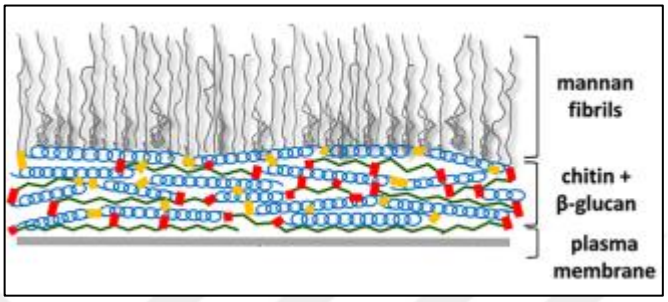

Figure 1.3. Schematic illustration of yeast cell wall [9]

1.2.1. Microbial Growth

Growth of microorganisms can be achieved when the parameters that affect the growth are optimized. Physical and chemical conditions are the most important parameters in microbial growth. Chemical conditions include the presence of water and energy source in the medium. In order to grow and increase the number of cells, microorganisms require some essential elements such as C, H, O_2 and N_2 and growth factors in the medium. Moreover, physical conditions such as temperature, osmotic pressure, and pH also have an important role in microbial growth. If all the conditions are optimized, microorganisms start their metabolic activity and as a result grow in size and number. When even a single microorganism encounters a new environment, following four phases of microbial growth take place. The first phase is named as lag phase and during this phase microorganisms try to adapt their new environment and synthesize necessary enzymes and proteins for their proliferation. After this adaptation step, the rate of DNA synthesis increases and as a result, cells begin to divide at their maximum rate. This second step is log phase, and the increase in number of cells can be observed in this phase clearly. Furthermore, due to increased metabolic activity, microorganisms become more sensitive to external factors such as antibiotics. When they reach a certain population size, they enter the third phase which is

stationary phase. This phase results from mostly depletion of a nutrient, and/or formation of inhibitory products. Also, synthesis of secondary metabolites occurs in this phase. If the conditions remain the same, rate of death becomes higher than rate of proliferation because of decreasing nutrient and microorganisms go their last phase which is named as death phase. Duration of growth phases may vary from species to species [10].

1.2.2. *Escherichia Coli*

Escherichia coli is a member of the family Enterobacteriaceae. It is a rod-shaped bacterium with 2.0 μm length and 0.25-1.0 μm diameter. The peptidoglycan layer of its cell wall is thin and stains pink with counterstain safranin which indicates that *E.coli* is a Gram-negative bacterium. Some strains of *E.coli* are considered as pathogenic while some of them are normal inhabitant of the gut of many animals. It is a well-studied model organism for Gram-negative bacteria due to its ability of reproduction at high rates and its adaptation to laboratory environment [11]. *E.coli* can grow in any medium that contains glucose, sodium chloride, magnesium sulphate, ammonium phosphate monobasic, potassium phosphate dibasic, and water. The optimum temperature for growth of *E.coli* is 37 ^{o}C. Cellular respiration of *E.coli* cells can be either aerobic (if O_2 is present) or anaerobic (if O_2 is absent). This trait increases the chances of survival of bacteria [12].

As a model organism, *E.coli* has been used in many different scientific areas such as genome-sequencing [13], metabolomics [14], and antimicrobial agent tests [15,16]. The last topic is extremely important in terms of understand the mechanism of toxicity of chemicals and agents towards pathogenic or non-pathogenic bacteria. Nano science and nanotechnology has recently become one of the most popular research areas. As a result, the variety of nanoparticles as well as their synthesis methods increases day by day. Toxicity of all these nanoparticles has been testing on different types of cells. *E.coli* is widely used in these toxicity tests. As an example, in the study of McQuillan *et al.* dissolution-based toxicity mechanism of silver nanoparticles to *E.coli* was investigated [17]. Similar studies including antibacterial activity of zinc oxide (ZnO) nanoparticles against *E.coli* [18], toxic effect of iron oxide nanoparticles on *E.coli* [19], and microbial toxicity of different metal oxide nanoparticles (CuO, NiO, ZnO and Sb_2O_3) on three

different microorganism (*Escherichia coli*, *Bacillus subtilis* and *Streptococcus aureus*) were done [20].

1.2.3. *Saccharomyces Cerevisiae*

Although there are many species of yeast, *Saccharomyces cerevisiae* is the microorganism that comes to mind in everyday language. *S.cerevisiae* has been widely used in daily fermentation processes such as making bread, wine and beer since the ancient times, making it one of the first domesticated organisms. In addition to its benefits to daily human life throughout history, it is one of the most suitable model organisms for eukaryotic systems. Due to its many advantages, studies have focused on this microorganism starting from the beginning of twentieth century. *S.cerevisiae* has been very useful for investigation of metabolic pathways, characterization of enzymes, and understanding signal transduction mechanisms [21]. Life cycle of *S.cerevisiae* alternates between asexual and sexual reproductive cycles. R. K. Mortimer and colleagues developed both meiotic and mitotic approaches and completed the genomic sequence of *S.cerevisiae* over the years [22].

As an eukaryotic cell, *S.cerevisiae* possesses all membrane-bound organelles (except chloroplasts) and a nucleus. Cell wall of yeast differs from bacterial cell wall and is composed of mannoproteins (highly glycosylated glycoproteins), β-glucans and chitin. Even if they have ability to follow two modes of reproduction, they reproduce by budding at normal conditions. When cells grow to a certain size, they form a bud on the cell wall and start DNA synthesis at the same time [21]. *S.cerevisiae* cells can produce ATP through either respiration and/or fermentation during growth. The availability of fermentable carbon sources such as glucose in the medium has a huge impact on the determination of which metabolic pathway will be chosen for ATP synthesis. Acetate, succinate, glycerol and ethanol are the byproducts of yeast fermentation and can be only used as carbon sources in mitochondrial respiration. Also, Olivares-Marin *et al.* compared the growth curves of cultures with different glucose concentrations. They concluded that when ATP is synthesized mainly through fermentation rather than oxidative phosphorylation, the culture reaches the log phase in a shorter time and high growth rates can be obtained during this phase [23]. The growth, metabolism and fermentation process of *S.cerevisiae* has been investigated and engineered in many ways especially in biotechnology field [24–27]. It is

also mainly used as an eukaryotic model organism in order to assess biocidal effect of nanoparticles [28–30].

1.3. SILVER NANOPARTICLES

Nanomaterials and nanotechnology have recently been used in many applications due to their novel electrical, catalytic, magnetic, photonic, and thermal properties compared to their macroscaled counterparts. Owing to these properties, many studies investigating their antimicrobial properties [31–33], their usage in drug delivery applications [34,35], and their contribution as substrates to spectroscopic techniques such as Surface-Enhanced Raman Spectroscopy (SERS) have been done [36,37]. Among nanoparticles, silver nanoparticles (AgNPs) draw attention due to their use in different research areas. Depending on their synthesis method, they exhibit different properties. One of the most popular properties of AgNPs is its biocidal effect against microorganisms. As a result of its antimicrobial effect, AgNPs are widely used in pharmaceutical and food industry, and also in water treatment [32]. When microorganisms are exposed to AgNPs, they can penetrate into the cells due to their small sizes. The release of Ag^+ ions from AgNPs results in direct contact of Ag^+ ions with phosphorus- or sulphur- containing biomolecules such as DNA, RNA, and proteins. Also formation of reactive oxygen species (ROS) by AgNPs damages the membrane of microorganisms [31]. The advantage of AgNPs over ionic silver is that the size and shape of AgNPs can be controlled meaning that their antimicrobial activity can be enhanced during synthesis of AgNPs [32].

There are many ways of synthesizing AgNPs such as using a ceramic heater that has a local heating area [38], using electrical spark [39], using microorganisms to reduce silver salts [40], but the most common way is reduction of silver ions by reducing chemicals. In this case many reducing chemicals such as sodium borohydride, hydrazine hydrate, sodium citrate, ascorbic acid [32] as well as some reducing sugars such as glucose, galactose, maltose, and lactose can be used. Different reducing agents and stabilizers have an effect on the size, size distribution, and morphology of nanoparticles [41].

1.3.1. Maltose-reduced AgNPs

Using a disaccharide as a reducing agent in the synthesis of AgNPs has some advantages over other reducing agents. As an example, Çulha *et al.* synthesized AgNPs by using only maltose monohydrate and tested its antimicrobial activity against a broad-spectrum of bacteria. As there is no need of any hazardous stabilizer such as polyvinylpyrrolidone (PVP) during synthesis, it can be said that this is a green-chemistry approach. A narrow size distribution can be also achieved by using maltose in the synthesis. Furthermore, biocidal activity of AgNPs is affected by both size and dissolution rate of nanoparticles. If a weak reducing agent is used for synthesis, the release of Ag^+ ion from AgNPs will be faster. Carbohydrates are weak reducing agents when compared with citrate or borohydrate. As a result, using a carbohydrate as reducing agent increases the release rate of Ag^+ ions thus increases antimicrobial activity of nanoparticle [42]. In another study, synthesis was done by using four different reducing sugars (glucose, galactose, maltose and lactose) and the antimicrobial activities of obtained AgNPs were tested. It was concluded that among all AgNPs, those synthesized by reducing with maltose showed the highest antimicrobial activity. Investigation of nanoparticles with greater biocidal effects on pathogenic microorganisms becomes more important, as the resistance of microorganisms to antibiotics increases due to their overuse [41]. It should also be noted that not every AgNPs synthesis method produce AgNPs with biocidal properties. For example, citrate reduced AgNPs (c-AgNPs) do not show almost any biocidal effect. Biocidal effect of c-AgNPs was tested against *Escherichia coli* and *Baccillus megaterium* by Kahraman *et al.* They checked the viability of bacterial cells after 30 minutes incubation with AgNPs colloidal suspension by re-culturing the bacteria on agar plates. Their results demonstrated that c-AgNPs have almost no toxic effect on microorganisms [43].

1.4. RAMAN SCATTERING AND SURFACE ENHANCED RAMAN SCATTERING

1.4.1. Theory of Raman Spectroscopy

In general, spectroscopy deals with interaction of electromagnetic radiation with matter. The aim of using different spectroscopy techniques is to obtain information about a compound's structure, composition, and properties. By using absorption and/or scattering phenomena, electronic structures and/or vibrational behaviour of a compound can be obtained. According to the frequency of absorbed radiation, energy levels of the compound can be determined. Also a quantitative data can be obtained from the intensity of absorption. Among many spectroscopic methods, vibrational spectroscopy is widely used in order to characterize compounds based on their molecular vibrations.

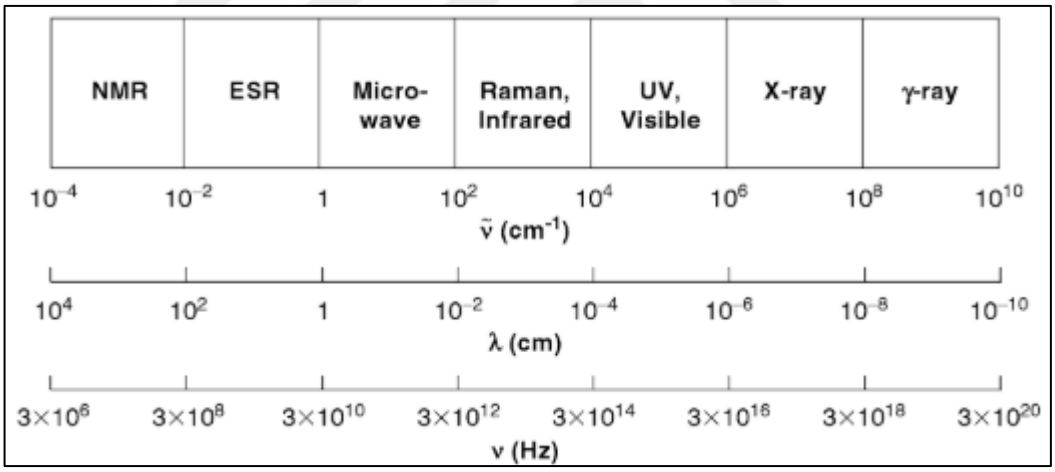

Figure 1.4. Electromagnetic spectrum and related energy units [44]

The vibrational displacements of molecules depend on the number of atoms in the compound as well as their linearity and symmetry. Total number of displacements of a molecule can be found by multiplying number of atoms by three. Translational, rotational, and vibrational motions contribute to these displacements. There are three translational motions for both linear and non-linear molecules. On the other hand, the number of rotational motions differs according to linearity of molecules. There are three rotational motions for non-linear molecules whereas for linear molecules this number decreases by one because there is no rotation around the axis. When translational and rotational motions

are subtracted from total number of displacements, number of vibrational motions can be found. Briefly, for a non-linear molecule it can be calculated as 3N-6 and for a linear molecule it can be calculated as 3N-5 where N is the number of atoms in the molecule. These vibrations are named as normal modes and can be either Infrared (IR) active or Raman active independently, but cannot be both according to the exclusion rule. If electric dipole moment of a molecule changes due to a normal mode, it can absorb infrared radiation and can contribute to IR spectrum which makes that particular normal mode IR active. Raman activity of normal modes is similar to IR activity but in this case polarizability changes due to distortion of a molecule [45].

Raman scattering was first observed by C.V. Raman and his colleague K.S. Krishnan in 1928 [46]. After that, identification of molecules has been done by measuring frequency and intensity of scattered radiations, and this technique named after its inventor, C.V. Raman. After an incident light in visible region of electromagnetic spectrum interacts with electron cloud of molecules, it polarizes the electron cloud and cause an excitation of electrons to a virtual state. But electrons in this state are not stable so electron cloud relaxes and photons scatter in all directions.

There are two possible types of scattering; radiation can be scattered elastically or inelastically. Rayleigh scattering occurs when the frequency of scattered radiation is equal to the frequency of incident radiation which results in an elastic scattering. Most of the scattered radiation occurs as this kind of scattering. But due to vibrations of molecules a shift in the frequency of scattered radiation can also be observed. This inelastic scattering of radiation is called as Raman Effect and can be collected to construct Raman spectrum. The frequency of scattered radiation can be either higher or lower than the frequency of incident radiation. If the frequency of scattered radiation is lower than the frequency of incident radiation, Stokes lines occur in the spectrum. This happens as a result of energy transfer from photon to the electrons of molecule. Molecule gains frequency thus scattered photon has lower frequency, energy, and wavenumber but it has higher wavelength. Another scenario may take place if the molecule is already at vibrational states when it absorbs a photon. In this case, molecule turns back to the ground state by transferring its excessive energy to the incident photon. This causes frequency and energy increase in the scattered radiation and can be visualized as anti-Stokes shift in the Raman spectrum [47,48].

The information gathered from Raman spectrum is very useful in terms of understanding molecular structures of materials. The shifts in wavelength are affected by force constants or bond distances of atoms. The frequency of vibration is determined by the inter-atomic force constant and vibrational intensities are related with polarizability of the electron cloud. Overall characteristic properties of vibrations result in bands at different wavenumbers on Raman spectrum, that are known as characteristic "*fingerprint bands*" of a molecule, making detection and identification of molecules easier [47].

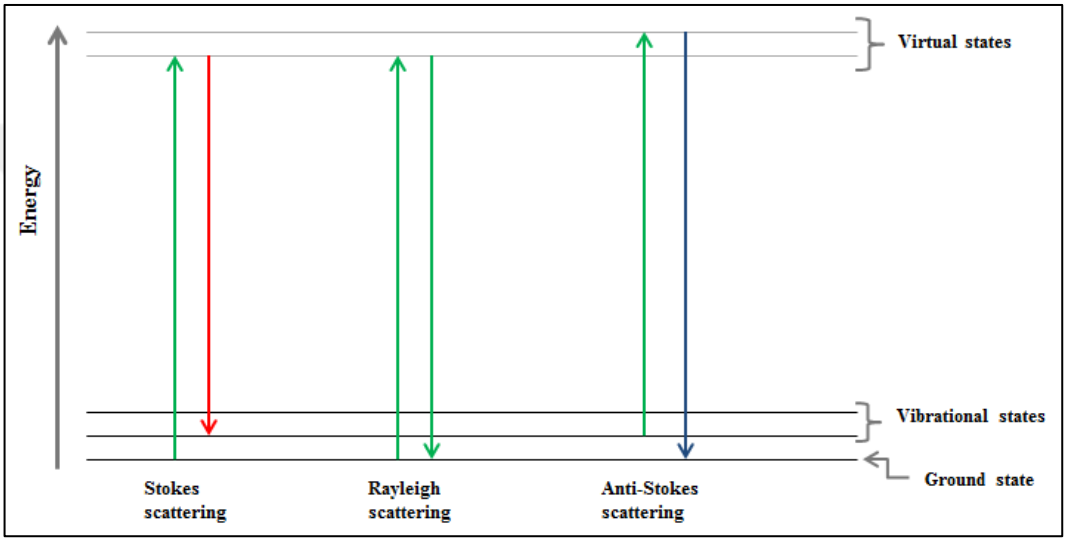

Figure 1.5. Schematic diagram of Rayleigh, Stokes and anti-Stokes scattering

1.4.2. Surface Enhanced Raman Spectroscopy

Raman spectroscopy has many advantages over the other spectroscopic methods. These advantages arise from ease of sample preparation, being non-destructive and having no interference with water and glass as they have very weak Raman spectra. On the other hand, the signals resulted from scattered photons have inherently weak nature. Applying high laser power and collection of scattering radiation for a long time can increase the intensity however it may cause decomposition of the sample at the same time. In order to increase the Raman intensity of vibrations, molecules can be brought into close vicinity of a nanostructured noble metal surface such as gold and silver nanoparticles [49].

When electromagnetic waves travel along conductor metal-dielectric interference, they couple with oscillating electron plasma of metal and this coupling generates surface plasmon polaritions (SPP). Only noble metals such as gold, silver, and copper support the formation of the plasmons. If the surface of noble metal is flat, the excited surface plasmons are called as surface plasmon resonance (SPR). If they are generated on nanostructured noble metal, they are called localized surface plasmons (LSPRs). LSPRs can enhance the intensity of Raman signals as high as 10^8 by forming intense electromagnetic area around scattered light. Another mechanism of enhancement can be a charge transfer between molecule and metal surface however it is thought that this mechanism is not as effective as electromagnetic effect. Phenomenon of LSPR was first applied to Raman spectrum of pyridine in 1974 by Fleischman *et al.* After that the strong relationship between electromagnetic enhancement and surface plasmons (SPs) was understood and this led many improvements in Raman spectroscopy [50].

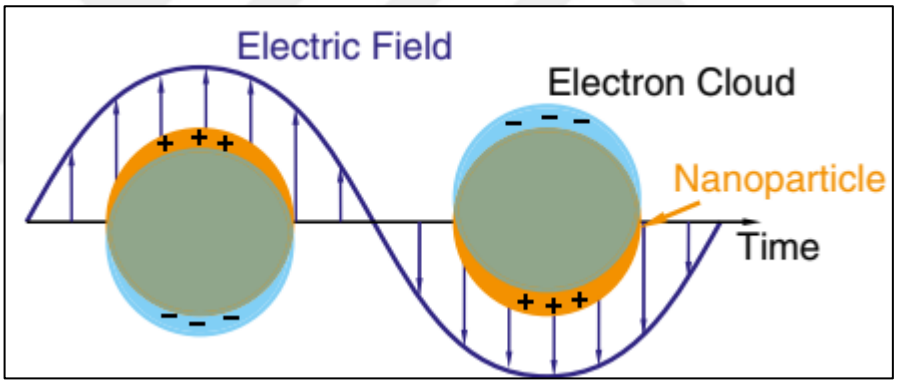

Figure 1.6. Schematic of localized surface plasmon resonance (LSPR) [51]

Gold nanoparticles (AuNPs) and AgNPs have been widely used as SERS substrates in sensing and imaging applications. The size, shape and aggregation tendency of nanoparticles as well as different reducing agents used in the synthesis have important effects on the performance of SERS. Researches have focused on optimizing these parameters. In a study, SERS activity of silver colloids prepared by reducing with different chemicals was tested. The best Raman enhancement was achieved with citrate-reduced AgNPs [52]. Therefore, c-AgNPs are one of the most used SERS substrates as their synthesis method is easy to conduct and the produced AgNPs have high SERS activity [53].

1.4.3. Application of SERS in Biological Samples

Using SERS in detection, identification, and monitoring of biological samples has become more popular owing to many advantages of the technique. Being insensitive to water molecules makes SERS an important tool in biological studies. Furthermore, signal enhancement with the help of LSPRs makes it possible to use low laser power and prevent destruction of biological samples. Finally, from sample preparation to obtaining and analysing the spectrum, SERS is a rapid method in comparison with other methods of analysis such as IR spectroscopy, mass spectroscopy, etc.

SERS can be applied in a wide range of applications such as imaging the cell wall of microorganisms [54,55], identification [56] and discrimination of different organisms [57], monitoring biofilm formation [58–61], profiling metabolites [62], detection of other biological macromolecules such as proteins [63], genetic material (DNA and RNA) [64], and detection of illicit drugs in forensic samples [48]. Another advantage of using SERS in detection and identification of microorganisms is low limit of detection (LOD) values. As an example, Ag@TiO_2 nanofibrous felts constructed by Yang *et al.* served as a SERS substrate with limit of detection as low as 10^{-9} mol/L [65]. Thus, it can be used in detection and monitoring of diseases [66–68], or can be coupled with other techniques in order to construct point-of–care biosensors (POC) [69,70].

Raman scattering is correlated with polarizability of electron clouds around nuclei, therefore double bonds with π-electron clouds are strong Raman scatters as they are easily distorted in an external electric field. Also they are prone to cause induced dipole moments by changing the distribution of electron density due to their bending or stretching vibrations [47]. The Raman intensity of polar organic bonds, such as C-O, N-O, and O-H, are weak whereas intensity of neutral bonds, such as C-C, C-H, and C=C, are strong [71]. This makes SERS a more advantageous analytical tool for studying biological samples, as cells, metabolites, and biological macromolecules are generally contain the bonds mentioned above. In a study, real-time changes during the cell cycle of a single yeast cell was monitored by analysing Raman peaks coming from m-RNA, proteins, and lipids [72]. In another study, in situ quantification of fermentation process was done by obtaining Raman spectra of fermentation components, such as, ethanol, glucose, glycerol, and lactic acid [73].

2. MATERIALS AND METHODS

2.1. MATERIALS

2.1.1. Chemicals

Tri-sodium citrate and maltose monohydtrate were purchased from Merck (Merck KGaA, Darmstadt, Germany). Silver nitrate ($AgNO_3$) (99.5 percent) and sodium chloride were purchased from Sigma-Aldrich. Sabouraud dextrose broth (SDB) and peptone from casein, pancreatic digest were obtained from Fluka. Yeast extract was purchased from BioLife. All chemicals were used as received without further purification.

2.1.2. Microorganisms

The microorganisms *Escherichia coli* ATCC 10536 and *Saccharomyces cerevisiae* ATCC 9763 were obtained from our microorganism collection (Yeditepe University, Genetics and Bioengineering Department).

2.2. EXPERIMENTAL DESIGN

As mentioned above, the growth of microorganisms is highly affected by their environment. Maltose-reduced AgNPs are known to decrease the viability of microorganisms through several mechanisms. This study investigates how the growth and metabolite profile of microorganisms is affected if m-AgNPs are present in their culture media. In order to make a comparison between prokaryotic and eukaryotic cells, two different microorganisms, *E.coli* as a bacteria and *S.crevisiae* as a yeast cell, were selected. In microbiology, UV/VIS spectrometry is widely used in order to measure the turbidity of medium. Turbidity or optical density (OD) of medium increases in accordance with increasing number of cells and can be used in order to observe microbial growth. Another spectroscopic method, surface-enhanced Raman spectroscopy, was used in order to

monitor the changes in the chemical components of the media, resulted from the metabolic activity of the cells, both in the presence and in the absence of m-AgNPs.

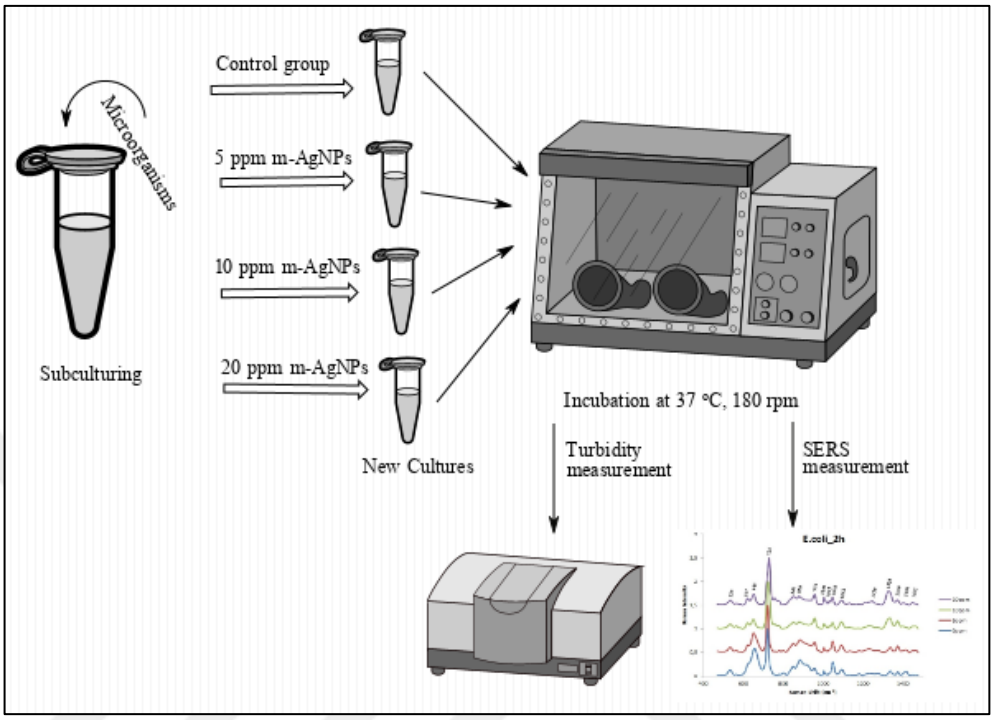

Figure 2.1. Schematic illustration of experimental design

Briefly, *E.coli* and *S.cerevisiae* cells were subcultured in their liquid media LB and SDB, respectively. Turbidity of subcultured cells was measured and necessary dilutions were done in order to obtain the same number of cells in the media at the beginning of the inoculation. Cells with their respective media were prepared in four different falcon tubes. Then, freshly prepared m-AgNPs were added into the media in order to obtain final concentrations of 5, 10, and 20 parts per million (ppm). They were incubated with m-AgNPs and samples were taken after certain incubation times (2, 6, 12, 24, and 48 hours of incubation) in order to measure optical density of media. Also, 5 μL of samples were mixed with c-AgNPs and was dropped on CaF_2 for SERS measurements.

In these set of experiments, the turbidity and SERS results of cell cultures that do not contain m-AgNPs were used as control experiment for both microorganisms. As the effect of m-AgNPs on growth was investigated, the results of control group was compared with the results of cell cultures that are prepared by mixing with 5, 10, and 20 ppm m-AgNPs.

2.3. METHODS

2.3.1. Synthesis of Citrate-Reduced Silver Nanoparticles

Citrate-reduced AgNPs were synthesized by well-known Lee and Meisel method [74]. Briefly, 90 mg of $AgNO_3$ was dissolved in 500 mL ddH_2O and the solution was heated under stirring until boiling. After the solution started boiling, 10 mL (1 percent) of filtered tri-sodium citrate solution was added drop wise into the solution. When the volume reduces to 250 mL due to boiling, the flask was taken from boiling and left to cool down to room temperature. The initial concentration of the prepared AgNPs colloidal suspension is referred as 1X. The 1X suspension was concentrated 4-times by centrifuging at 5500 rpm for 30 min, removing ¾ of the supernatant and resuspending, and named as 4X, which was used for the SERS measurements. The characterization of c-AgNPs was done by using UV/VIS spectroscopy and Dynamic Light Scattering (DLS). Furthermore, SERS spectra of c-AgNPs were obtained in order to check whether there is any interference coming from c-AgNPs on the spectra or not.

2.3.2. Synthesis of Maltose-Reduced Silver Nanoparticles

Maltose-reduced AgNPs were synthesized by a previously reported method [42]. 50 grams of maltose was dissolved in 100 mL of ddH_2O and was heated to boil. Meanwhile, $AgNO_3$ solution was prepared by dissolving 0.475 grams of $AgNO_3$ in 2 mL of ddH_2O. When the maltose solution started to boil, prepared $AgNO_3$ solution was added into the maltose solution drop wise. After $AgNO_3$ solution was added, the solution was boiled for 2 more minutes then put directly into ice bath to decrease the temperature which terminates the reaction.

2.3.3. Construction of Growth Curves of Microorganisms

E.coli and *S.cerevisiae* were sub-cultured at 37 ^{o}C for 16 hours in LB (Yeast extract 5 g/L; Peptone from pancreatic digestion 10 g/L; NaCl 10 g/L) and SDB, respectively. In order to construct the growth curve of *E.coli* and *S.cervisiae*, their optical density (OD) was

measured at 600 nm. Then, fresh cultures for both cells were prepared with 0.02 initial ODs and their ODs were measured from 2 to 55 hours. Similarly, in order to observe growth profile in the presence of m-AgNPs, *E.coli* and *S.cervisiae* were sub-cultered at 37 ^{o}C for 16 hours, then the initial ODs were adjusted equal for liquid media containing 5, 10, and 20 ppm m-AgNPs and for control group without m-AgNPs. *E.coli* and *S.cerevisiae* cells were incubated at 37 ^{o}C and OD_{600} of cells were measured at the end of 2, 6, 12, 24, and 48 hours of incubation. Logarithm of measured OD values were plotted against time in order to obtain growth profiles in the presence of m-AgNPs.

2.3.4. Preparation of Microorganism Samples for SERS Measurements

Prior to the experiment *E.coli* and *S.cerevisiae* were sub-cultured at 37 ^{o}C for 16 hours in LB and SDB, respectively. Fresh cell cultures, which contains 5, 10, 20 ppm m-AgNPs, were prepared by using the necessary amount of cells from primary culture. They were incubated at 37 ^{o}C until 48th hour and 5 µL of samples were collected at 2nd, 6th, 12th, 24th, and 48th hours. These samples were mixed with previously synthesized 4x c-AgNPs by mixing 5 µL of sample with 5 µL of c-AgNPs, and dropped on CaF_2 slide. Right after the drops were dried their SERS spectra were obtained.

2.3.5. Characterization of AgNPs

2.3.5.1. Ultraviolet-Visible Spectroscopy Analysis

A Perkin Elmer Lambda 25 Ultraviolet-Visible (UV-Vis) spectrometer was used in the characterization of c-AgNPs colloidal suspension and m-AgNPs. In order to construct the growth curves of microorganisms, the optical density (turbidity) measurements were performed at 600 nm wavelength with UV-VIS spectrometer.

2.3.5.2. Dynamic Light Scattering Analysis

The size of both c-AgNPs and m-AgNPs were performed using Malvern Zetasizer Nano ZS which is equipped with a 633 nm 4 mW He-Ne laser. Standard disposable polystyrene cuvettes were used for size measurements.

2.3.6. SERS Measurements

The SERS spectra were recorded using a Renishaw InVia Reflex Raman Microscopy system (Renishaw Plc., New Mills, Wotton-under-Edge, UK) equipped with a 830 nm diode laser and with a high speed encoded stage (Streamline^{TM}), a Leica DM2500 upright microscope. A 20x short distance objective with 2.5 μm spot size was used and 3 mW laser power was exposed to the samples for 10 seconds of exposure time. The system was automatically calibrated against a silicon wafer band at 520 cm^{-1}. From one spot, total of 36 spectra were obtained and for one sample, SERS spectra were collected from three different spots. So total of 108 spectra were collected from one sample. Samples were collected at designated incubation times. Also, SERS spectra of LB and SDB media were obtained in order to monitor how the concentrations of chemicals change with time.

3. RESULTS AND DISCUSSION

3.1. CHARACTERIZATION OF SILVER NANOPARTICLES

3.1.1. Characterization of c-AgNPs

The synthesized c-AgNPs were characterized with UV/VIS spectroscopy (Figure 3.1a) and Dynamic Light Scattering (Figure 3.1b). The maximum surface plasmon absorption of c-AgNPs was observed at 420 nm. According to DLS result, the size of c-AgNPs was obtained around 100 nm. These results are in accordance with the previous studies [75].

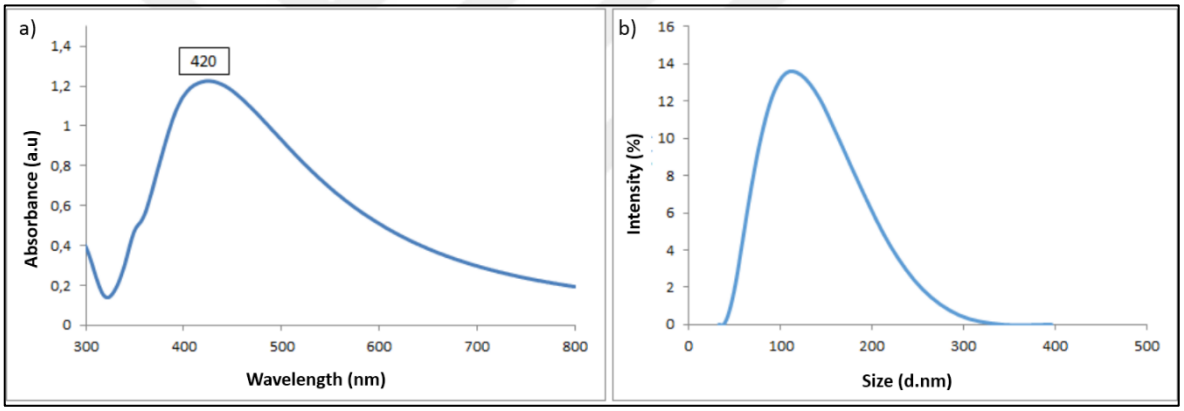

Figure 3.1. The results of c-AgNPs characterization a) UV/VIS spectrum of c-AgNPs and b) Dynamic Light Scattering (DLS) spectrum of c-AgNPs

3.1.2. Characterization of m-AgNPs

AgNPs, which were reduced by maltose, were characterized with UV/VIS spectroscopy (Figure 3.2a) and Dynamic Light Scattering (Figure 3.2b). The typical surface plasmon resonance absorption band at 420 nm can be seen on the UV/VIS spectrum of m-AgNPs. According to DLS result, the size of m-AgNPs was obtained around 20 nm with narrow size distribution. These results are in accordance with the previous studies [42].

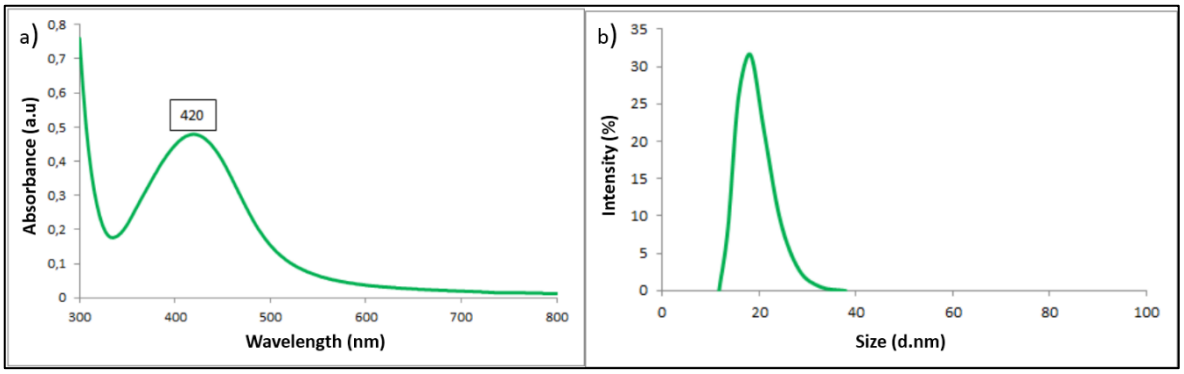

Figure 3.2. The results of m-AgNPs characterization a) UV/VIS spectrum of m-AgNPs and b) Dynamic Light Scattering (DLS) spectrum of m-AgNPs

3.2. GROWTH CURVES OF MICROORGANISMS

Optical density (OD) or turbidity is widely used in order to observe growth profile and growth rate of microorganisms. It is a very simple and rapid method to measure the proliferation of cells with the help of a UV/VIS spectrometer. Basically, cell density is measured with respect to a blank solution (in this case liquid media) by illuminating a light beam through sample and measuring the amount of absorbed photons. OD of cells increases with the increasing number of the cells. Plotting OD with respect to time gives the growth curve of microorganisms.

In this study, the growth profiles of both *E.coli* and *S.cerevisiae* were constructed prior to incubation with m-AgNPs. The ODs of both microorganisms were measured repeatedly from 0 to 55 hour. Then log number of OD versus time graph was plotted. In Figure 3.3 it can be seen that the obtained graphs are similar to typical growth curve graphs of bacteria and yeast cells.

After that, the growth of both cells was monitored in the presence of m-AgNPs. The effect of different concentrations of m-AgNPs on *E.coli* and *S.cerevisiae* cells was investigated. In a previous study, minimum inhibition concentrations (MIC) of m-AgNPs against different types of bacteria were demonstrated and the results were found between 1.69 and 13.5 ppm [41]. In our study, similar concentration values were used. Both cells were incubated with 5, 10, and 20 ppm m-AgNPs and a control group that does not contain any

m-AgNPs was prepared. At the beginning of incubation, OD values of cultures were arranged to be equal. ODs were measured and semi logarithmic graph of OD against time was plotted.

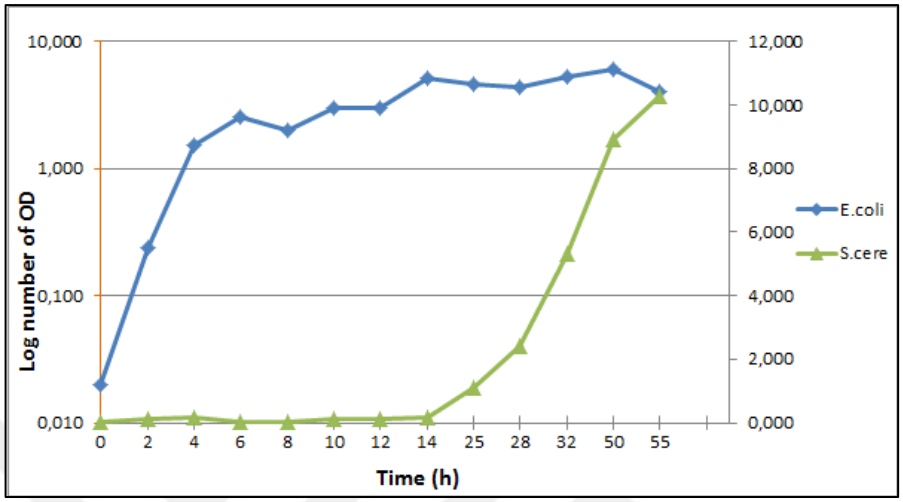

Figure 3.3. The growth profile of *E.coli* and *S.cervisiae* at OD_{600}

According to OD results, the growth of *E.coli* and *S.cerevisiae* is highly affected by the presence of m-AgNPs. In Figure 3.4, it can be seen that 5 ppm m-AgNPs caused a fluctuation in the growth of *E.coli* but the cells managed to proliferate especially after 24 hours of incubation. 10 ppm m-AgNPs concentration inhibits bacterial growth mostly but the initial OD value remain constant during 48 hours of incubation meaning that the cells could not proliferate but at least remained alive. When it comes to 20 ppm m-AgNPs concentration, it can be clearly seen that, m-AgNPs have a strong biocidal effect on *E.coli* at this concentration. Number of cells started to decrease right after their incubation with m-AgNPs at this concentration value.

In Figure 3.5 the effect of m-AgNPs on *S.cerevisiae*, Baker's yeast cell, is given. According to the graphs, a decrease in the cell density until 12 hour can be observed. After that the culture moves to log phase and the number of cells started to increase. However it can be said that the microbial growth was suppressed with respect to control group which has higher OD values. Still, *S.cerevisiae* cells could grow to a certain value unlike *E.coli* cells. The number of cells at the end of 48 hours of incubation was equal for 5 and 10 ppm m-AgNPs. This number decreases for 20 ppm concentration. The overall results of growth curves indicate that although m-AgNPs have more severe effects on *E.coli* than

S.cerevisiae, they suppressed the growth of both microorganisms at 20 ppm of m-AgNPs concentration. As OD data do not represent any information about the changes in the environment, detailed research was conducted with SERS in order to monitor these changes in the media due to the biocidal activity of m-AgNPs.

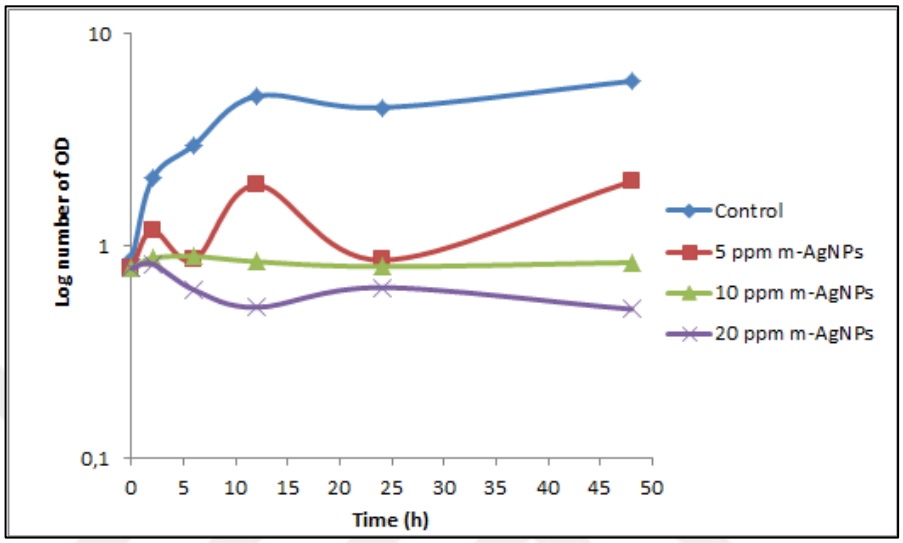

Figure 3.4. The growth curve of *E.coli* in the presence of 5, 10, and 20 ppm m-AgNPs

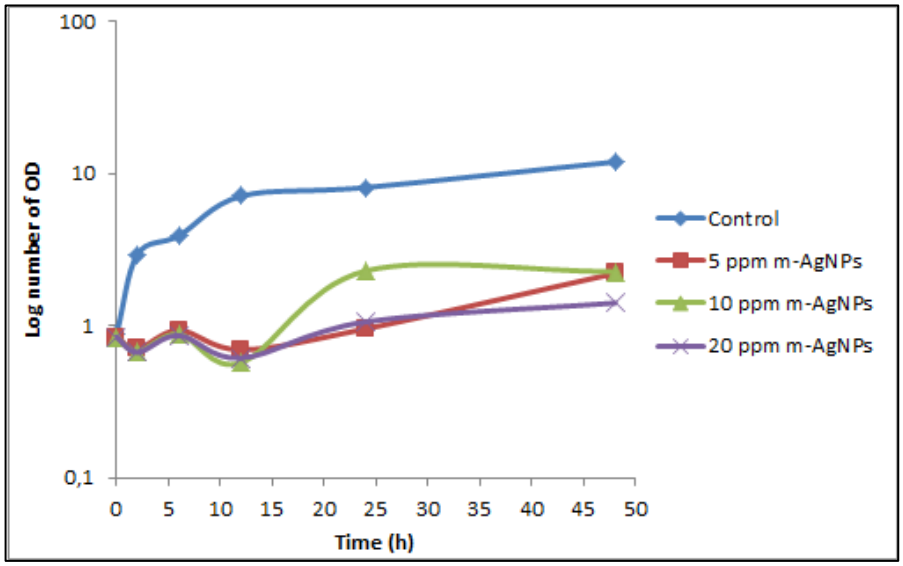

Figure 3.5. The growth curve of *S.cerevisiae* in the presence of 5, 10, and 20 ppm m-AgNPs

3.3. BACKGROUND SERS SPECTRA OF CITRATE REDUCED SILVER NANOPARTICLES

In order to detect any possible interference from the background, the SERS spectrum of c-AgNPs were obtained. Characteristic stretching peak of citrate can be seen at 1054 cm^{-1} on the SERS spectrum in Figure 3.6. This result shows that there is almost no interference coming from c-AgNPs.

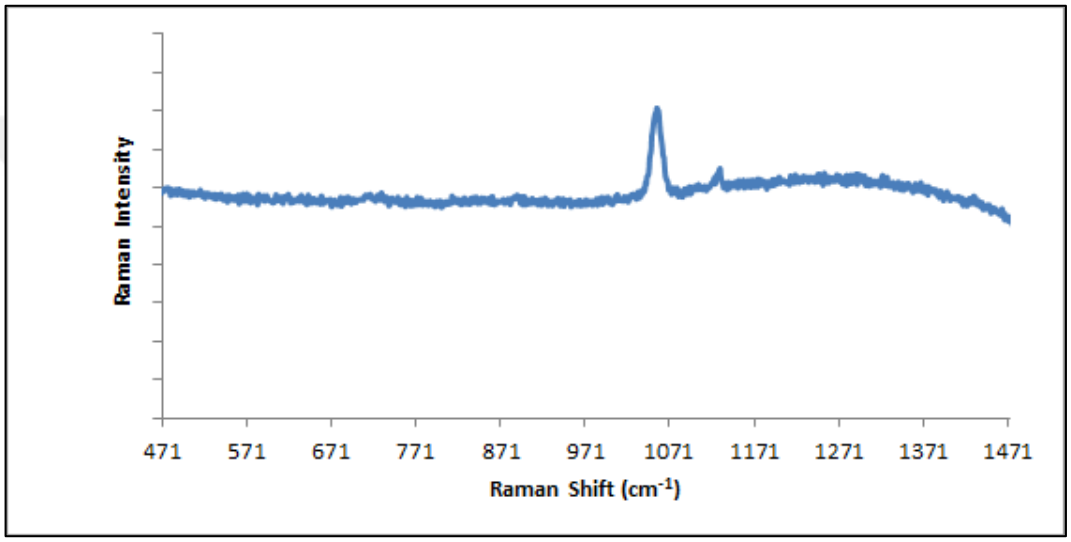

Figure 3.6. The SERS spectra of c-AgNPs

3.4. OBSERVATION OF MICROBIAL GROWTH FROM SERS SPECTRA

The growth profiles of *E.coli* and *S.cerevisiae* were investigated by monitoring the changes on SERS spectra due to changing cell number and environment. In order to detect the chemical changes resulted from metabolic activity, samples were taken from cell cultures of *E.coli* and *S.cerevisiae* at certain incubation times, and mixed with c-AgNPs without applying a washing step. Also, in order to distinguish the differences resulted from metabolic activity, the SERS spectra of media (LB for *E.coli* and SDB for *S.cerevisiae*) were obtained. The spectra were plotted as Raman intensity versus wavenumber. The increase or decrease in the constituents of environment, which are mostly biological macromolecules and organic compounds, results in changes in the peak intensity or causes a shift in the wavenumber.

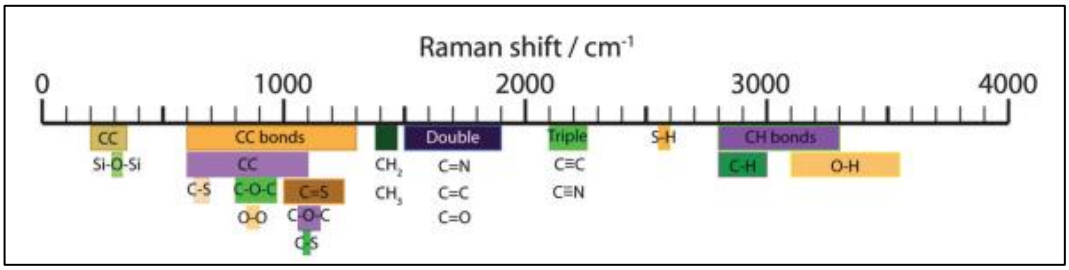

Figure 3.7. Raman shift ranges for organic molecules [71]

Table 3.1. List of tentative peak assignments for SERS spectra

Peak (cm^{-1})	**Assignment**
493	Polysaccharides [58]
506-528	S-S bond stretching [76]
560	C-S-S-C [77]
570-583	Carbohydrates [58]
613-620	COO- bending [77]
640-650,835-850	C-S stretching and C-C twisting of proteins (Tyrosine) [58,78]
710-730	Adenine from flavin (FAD) [77]
750-795	DNA/RNA fragments [78,79]
865-870	-C-C stretching and C-O-C 1,4-glycosidic link from carbohydrates [78,80]
900-914	C-COO- stretching from carbohydrates [81]
950-955	Possibly α-helices and/or carbohydrates [82]
965-966	C-N stretching [77]
1000	C-C aromatic ring stretching (Phenylalanine) [58]
1025-1031	Tryptophan [83]
1040-1085	C-O and C-C stretching of carbohydrates [78]
1080,1087	PO_2^- in nucleic acids [56]
1115-1120	Benzoid ring deformation [84]
1161	N-H of protein [58]
1166-1182	C-H bending of tyrosine [56]
1200-1203, 1225-1287	Amide III [58,77,85]
1318-1320	C-H bending from proteins [77]
1337-1408	COO- stretching of carbohydrate [86]
1435-1437	CH_2 defect [87,88]
1450-1462	CH_2CH_3 deformation of lipids and collagen [89]

3.4.1. Monitoring Growth of *E.coli* by using SERS

First of all, the SERS spectra of LB were obtained as background spactra in order to monitor the changes in *E.coli* cell culture with respect to time. LB without m-AgNPs and LB containing three different concentrations of m-AgNPs were mixed with c-AgNPs, dropped on CaF_2 slide and was left to dry. Three different areas on the drop were mapped during SERS measurements. According to Figure 3.8, there are many peaks coming from the ingredients of LB medium; peaks attributed to peptides [950 cm^{-1} (possible α-helices from proteins), amide III band at 1232 cm^{-1}, 1318 cm^{-1} (C-H bending from proteins), and 1437 cm^{-1} (CH_2 defect)], amino acids [S-S bond stretching at 522 cm^{-1}, 644 cm^{-1} and 840 cm^{-1} (peaks attributed to tyrosine), phenylalanine at 1000 cm^{-1}, and tryptophan at 1025 cm^{-1})] and carbohydrates [COO- bend at 614 cm^{-1}, 870 cm^{-1} (-C-C stretching, C-O-C 1,4-glycosidic link) and 1040 cm^{-1} (C-O and C-C stretching)] can be seen on the spectra of LB medium. In Figure 3.8, it can be seen that the concentration of m-AgNPs in LB does not have an effect on the SERS spectra, as exactly the same peaks were obtained for all concentrations. The strongest peak seen in LB spectra is at 727 cm^{-1} and attributed to adenine from flavins, which is found in vitamin B2 [77].

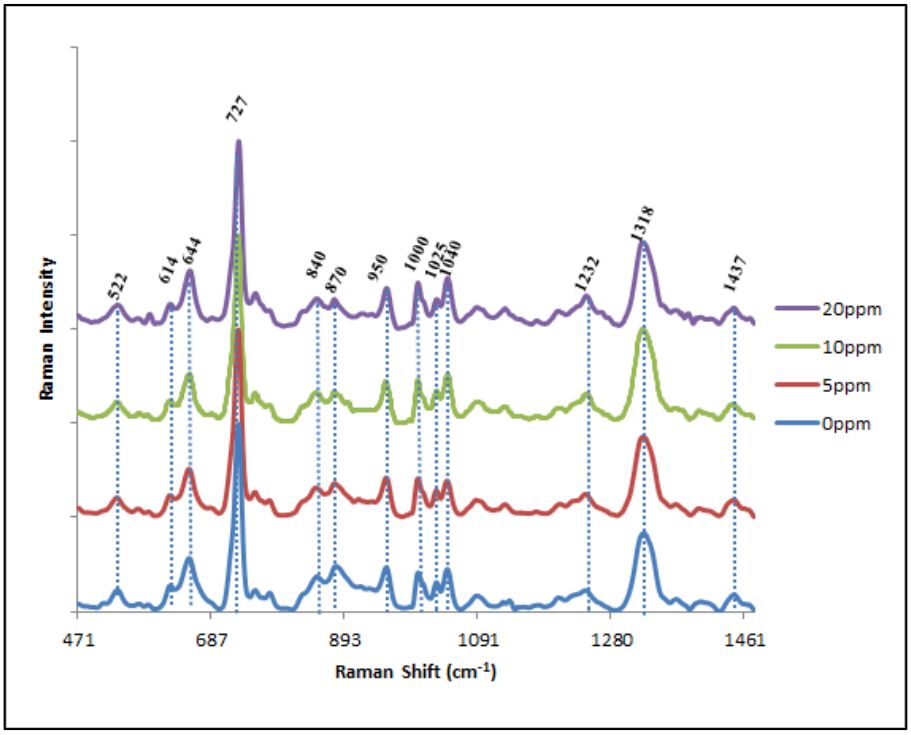

Figure 3.8. The SERS spectra of LB with different concentrations of m-AgNPs

The SERS spectra of cellular culture after 2 hours of incubation with LB medium that contain different amounts of m-AgNPs is given in Figure 3.9. Significant increase in the bands related to carbohydrates indicates synthesis of carbohydrates as a result of metabolic activity which is observed only for control group and *E.coli* incubated with 5 ppm m-AgNPs. In the spectrum of control group and 5 ppm m-AgNPs treated *E.coli*, the bands 645 cm^{-1} and 840 cm^{-1} (attributed to tyrosine) are increased. The concentration of tyrosine may increase due to hydrolysis of peptides in order to use them as building blocks during growth. In these two spectra, a decrease in the peak coming from C-H bending of proteins (1320 cm^{-1}) when compared with the spectra of LB medium, supports that protein content of the medium is used in microbial activity. In accordance with this, peak at 950 cm^{-1} band, which indicates α-helices coming from proteins, slightly decreased in the spectrum of the control group. According to the spectra of *E.coli* incubated with 10 and 20 ppm m-AgNPs, microbial growth is precluded at these concentrations as their spectra remained similar to LB medium after two hours of incubation.

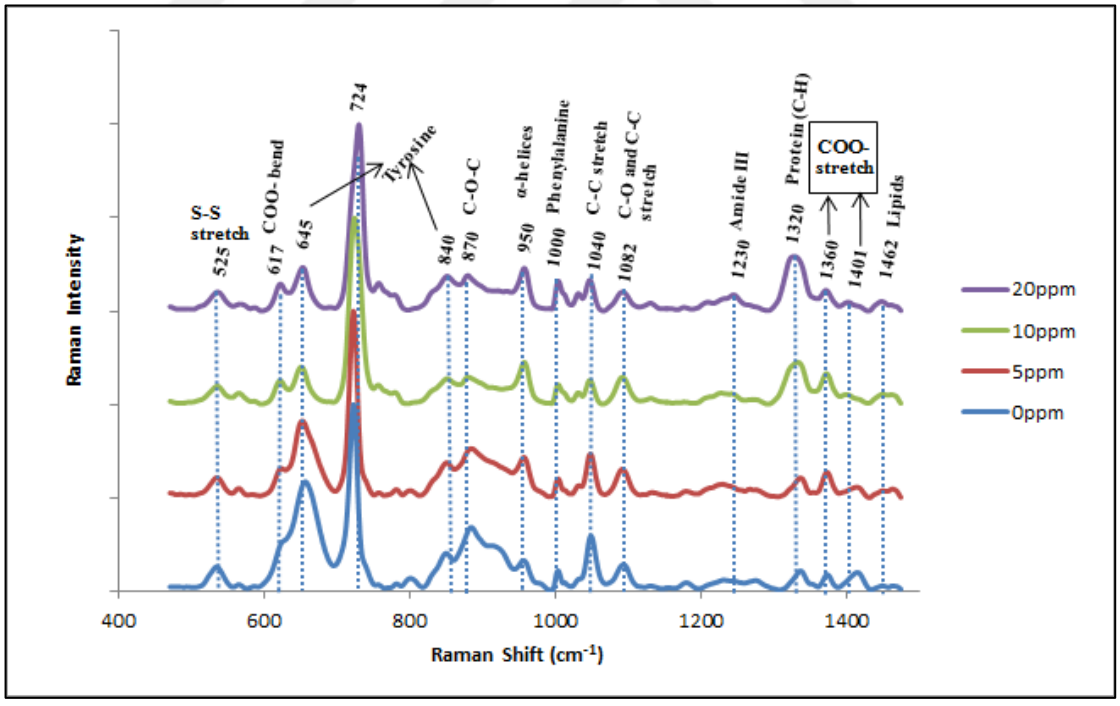

Figure 3.9. The SERS spectra of *E.coli* after 2 hours of incubation with different concentrations of m-AgNPs

When the spectra after 6 hours of incubation is investigated in Figure 3.10, it can be seen that carbohydrate content of *E.coli* treated with 10 ppm m-AgNPs has slightly increased

and the peak intensities are closer to control group of *E.coli* and *E.coli*/5 ppm m-AgNPs mixture at 2nd hour. Also an increase at tyrosine peak (644 cm^{-1}) can be seen. It can be said that *E.coli* cells were able to start their metabolic activity in 10 ppm m-AgNPs containing medium after 6 hours of incubation. Due to hydrolysis of peptides in the media, peak at 950 cm-1 which is attributed to α-helixes disappeared and also C-H bending peak of peptides at 1320 cm^{-1} decreased. Amide III band near 1258 cm^{-1} and an increase in S-S stretching band near 525 cm^{-1} can be seen in the spectra of the control and *E.coli*/5 ppm m-AgNPs group. The shift in amide III band (from 1230 cm^{-1} to 1258 cm^{-1}) may result from formation of disulfide bridges in the proteins or enzymes that are synthesized by the cells.

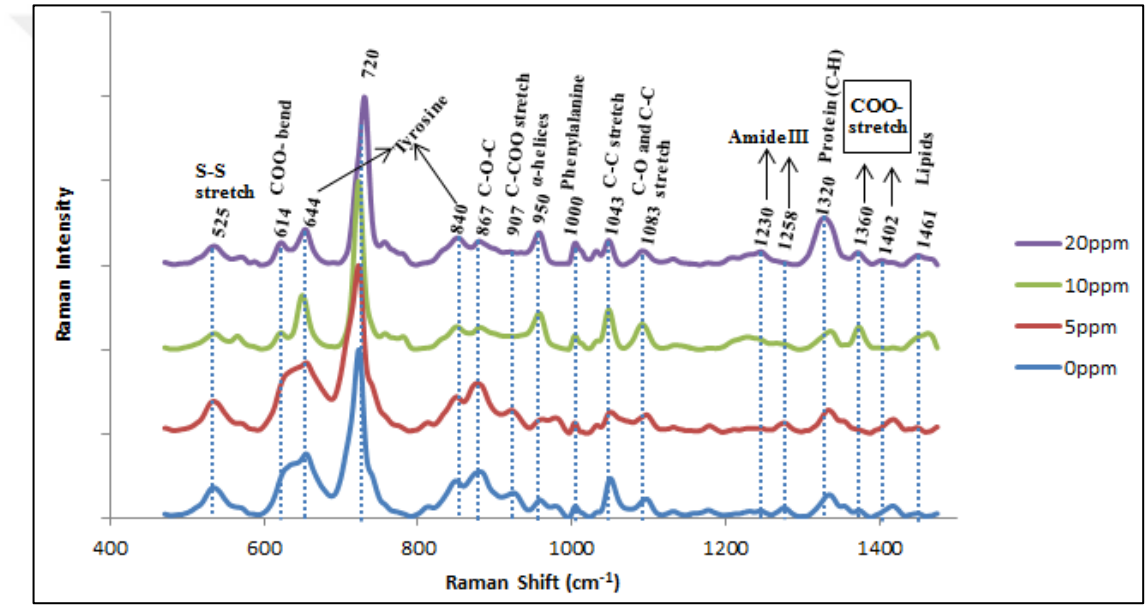

Figure 3.10. The SERS spectra of *E.coli* after 6 hours of incubation with different concentrations of m-AgNPs

In Figure 3.11 the SERS results of 12 hours of incubation can be seen. According to the SERS spectra, carbohydrate peaks in the spectrum of *E.coli* incubated with 10 ppm m-AgNPs reached their maximum and peaks in the spectra of control group and *E.coli*/5 ppm m-AgNPs remained almost same or decreased slightly. The latter can be the result of reaching the stationary phase in the cultures of control group and *E.coli*/5 ppm m-AgNPs [90]. Also Amide III bands and a dramatic increase in S-S stretching band can be observed in the spectrum of *E.coli*/10 ppm m-AgNPs after 12 hours of incubation. The formation of C-N stretching peak at 966 cm^{-1} may attributed to protein containing structures such as

peptidoglycans, which are one of the main components of bacterial cell envelope [91]. This peak can be seen on all spectra except *E.coli* cells treated with 20 ppm m-AgNPs. It can be related with increasing number of cells. A small increase at 1118 cm^{-1} originates from benzoid ring deformation.

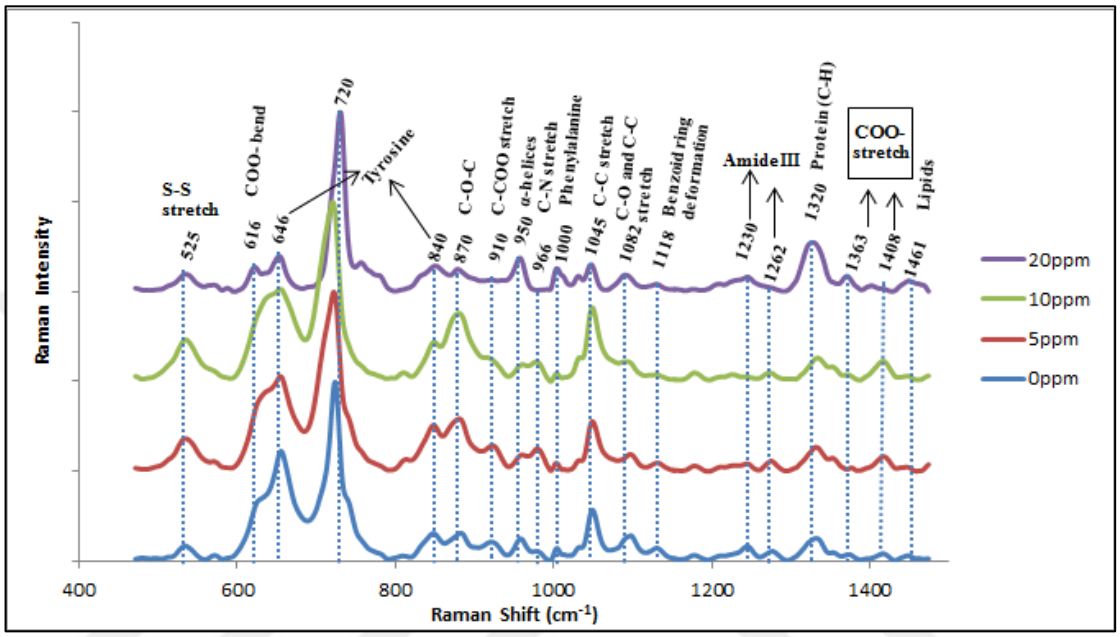

Figure 3.11. The SERS spectra of *E.coli* after 12 hours of incubation with different concentrations of m-AgNPs

In Figure 3.12 it can be seen that, intensities of peaks related with carbohydrates slightly decreased in the spectra of *E.coli*/5 ppm m-AgNPs and *E.coli*/10 ppm m-AgNPs at the 24th hour of incubation, meaning that metabolic activity decreased due to saturation of cells in the medium. In the spectrum of control group, it can be seen that the peaks attributed to carbohydrates and proteins increased when compared with the spectrum at 12th hour in Figure 3.11. This may be the result of disintegration of cells and releasing of their metabolites to the medium.

According to the SERS spectra of *E.coli*/5 ppm m-AgNPs and *E.coli*/10 ppm m-AgNPs after 48 hours of incubation in Figure 3.13, it can be said that their carbohydrate and protein peaks increased again as a result of cell disintegration. For control group, most of the peaks has decreased or diminished. No change in the spectrum of *E.coli*/20 ppm m-AgNPs with respect to the spectra of its medium is observed during 48 hours of incubation.

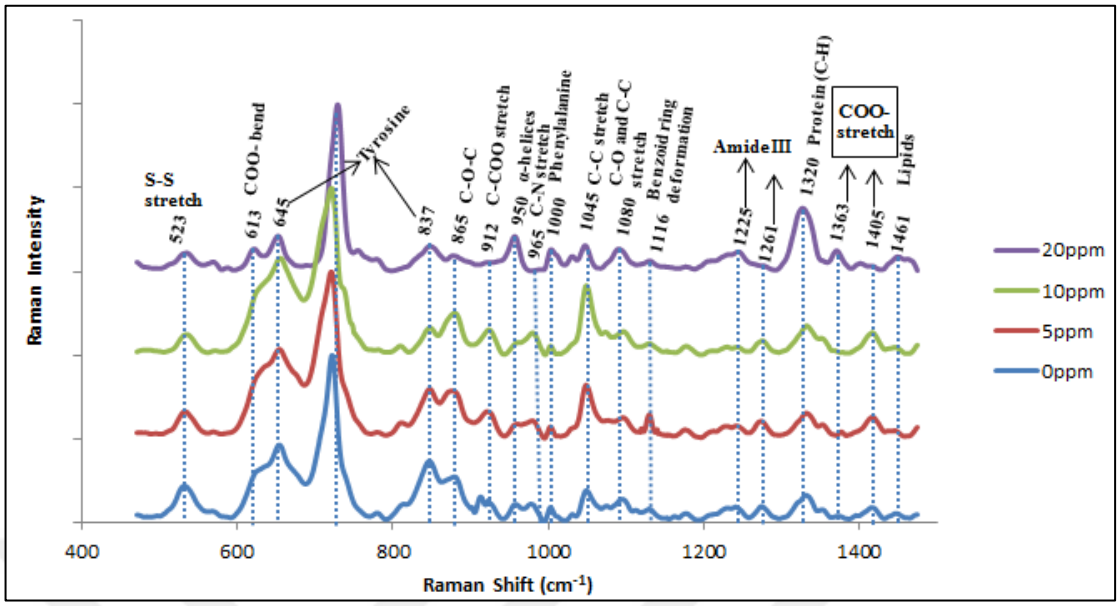

Figure 3.12. The SERS spectra of *E.coli* after 24 hours of incubation with different concentrations of m-AgNPs

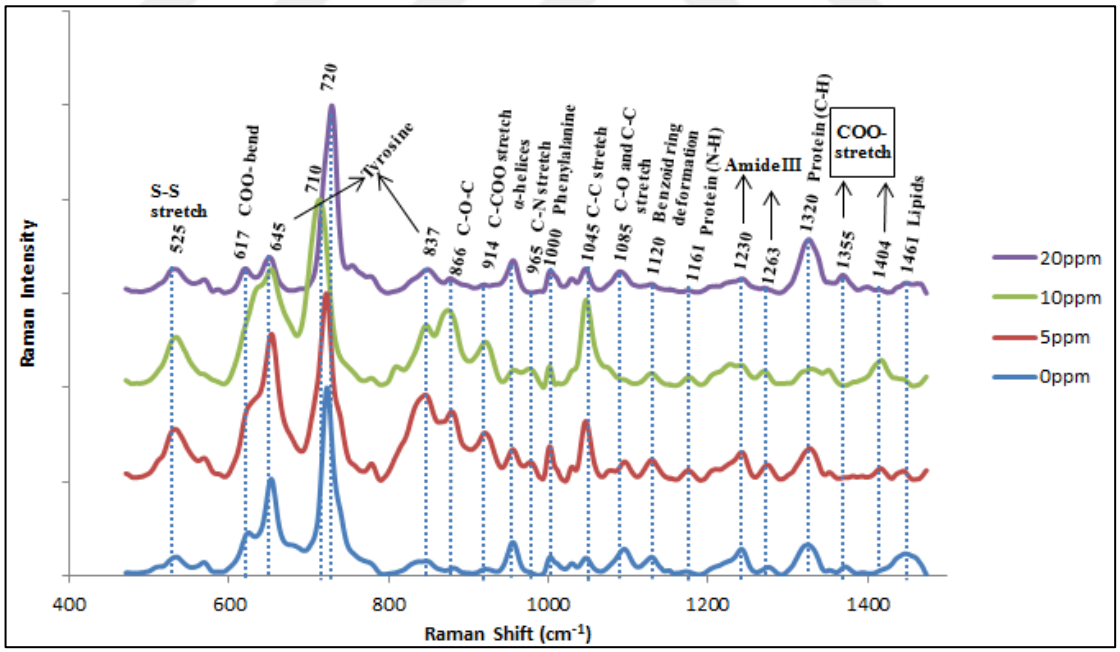

Figure 3.13. The SERS spectra of *E.coli* after 48 hours of incubation with different concentrations of m-AgNPs

According to all the SERS spectra obtained during 48 hours of incubation, it can be clearly stated that microbial growth of *E.coli* is suppressed in the presence of m-AgNPs. However,

the concentration of m-AgNPs has an important effect on this phenomenon. The concentration of 20 ppm m-AgNPs was enough to prevent the growth of *E.coli*. But the same statement cannot be done for 5 and 10 ppm m-AgNPs. Metabolic activity is observed at these concentrations with a decreasing rate. It can be said that the proliferation of cells, which are incubated with 10 ppm m-AgNPs, started at the 6^{th} hour by checking the peak intensities related with metabolites.

3.4.2. Monitoring Growth of *S.cerevisiae* by using SERS

On the purpose of the observation of effect of m-AgNPs on *S.cerevisiae* (yeast) cells, the SERS spectra of SDB (with three different concentrations of m-AgNPs and without m-AgNPs) were obtained as background spectra. 5 μL of samples were mixed with 5 μL of c-AgNPs and 5 μL of this mixture was dropped on CaF_2 slide. As soon as the drop dried, the SERS spectra were obtained from three different areas on the drop by mapping method.

Sabouraud Dextrose Broth (SDB) was used for cultivation of *Saccharomyces cerevisiae*, Baker's yeast. SDB consists of peptones and dextrose. The effect of m-AgNPs on *S.cerevisiae* cells were investigated by mixing the cells with SDB containing three different concentrations (5, 10 and 20 ppm) of m-AgNPs and SDB without any m-AgNPs was used as a control group. The SERS spectra of SDB media are given in Figure 3.14. The spectra show that the presence of m-AgNPs has no effect on SDB spectrum. The peaks related with carbohydrates (614 cm^{-1} and 900 cm^{-1}), peptides (510 cm^{-1}, 522 cm^{-1}, 950 cm^{-1}, 1232 cm^{-1}, and 1318 cm^{-1}), and amino acids (640 cm^{-1}, 835 cm^{-1}, and 1031 cm^{-1}) in SDB can be seen on the spectra. Also peaks attributed to adenine (727 cm^{-1}) and lipid (1450 cm^{-1}) is shown. Lastly, benzoid ring deformation can be observed at 1116 cm^{-1}.

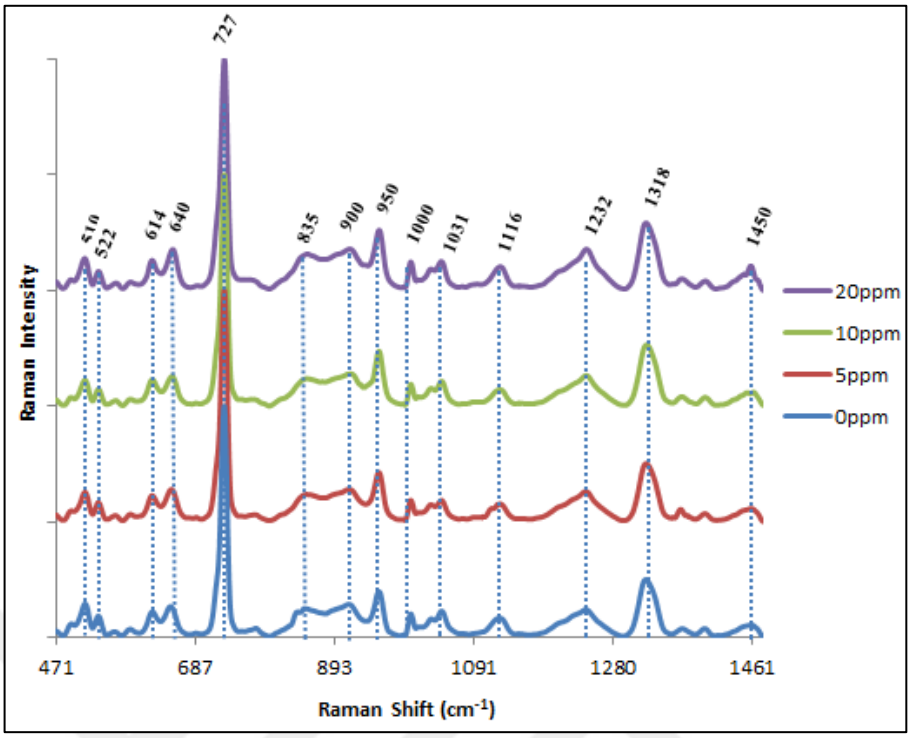

Figure 3.14. The SERS spectra of SDB with different concentrations of m-AgNPs

The SERS spectra after 2 hours of incubation can be seen in Figure 3.15. After 2 hour of cultivation, the peaks remain mostly similar to the spectra of corresponding medium. This is an expected result as the growth rate of yeasts are lower than most of the bacteria. Only the peaks related to tyrosine (648 cm^{-1} and 845 cm^{-1}), C-C stretching (1040 cm^{-1}) and amide III band (1232 cm^{-1}) increased slightly. This indicates the hydrolysis of peptides in the media and formation of enzymes for the growth. These spectra show the lag phase of cell culture in which cells are adapted to environment and prepared for growth [92]. Also a small peak of COO- stretching attributed to carbohydrates at 1360 cm^{-1} can be seen after 2 hours of cultivation. There is no significant difference for different concentrations of m-AgNPs at this incubation time.

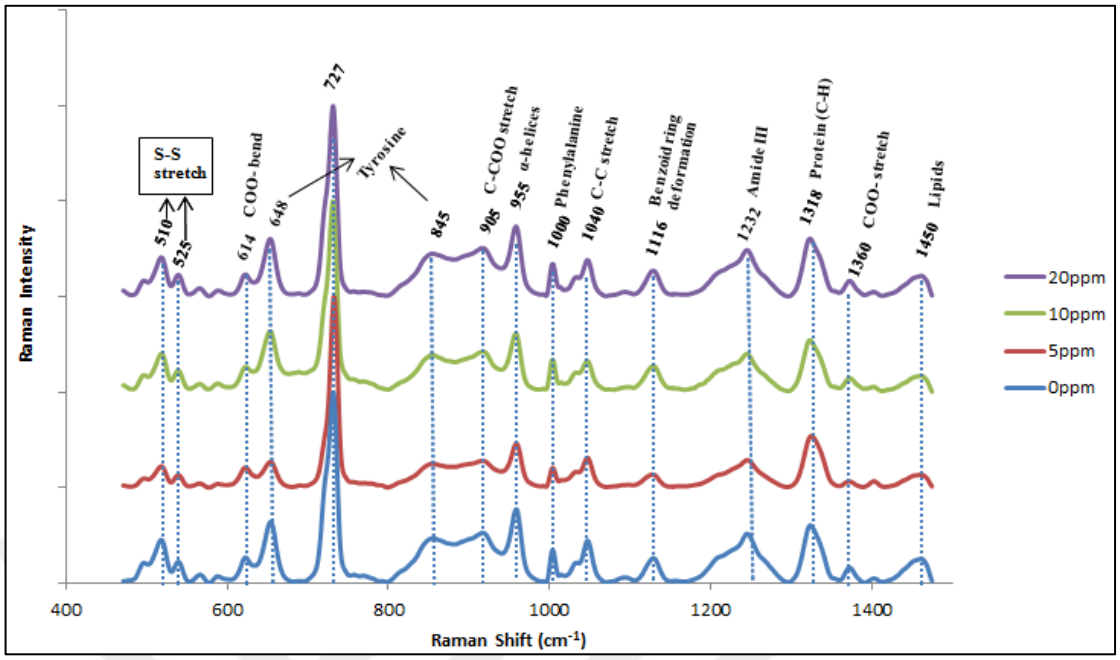

Figure 3.15. The SERS spectra of *S.cerevisiae* after 2 hours of incubation with different concentrations of m-AgNPs

In Figure 3.16., it can be seen that after 6 hours of incubation, many spectral changes occur in the spectra of samples containing 5 and 10 ppm m-AgNPs and also in the spectrum of control group. Peaks attributed to carbohydrates (493 cm^{-1}, 583 cm^{-1}, 908 cm^{-1}, 1045 cm^{-1} and $1340^{-1}405$ cm^{-1} bands) increased. This can be result of metabolic activity (for example, synthesis of polysaccharides from its monomers) of the yeast cells. The intensity of peaks related to disulfide bonds (at 515 cm^{-1} and 528 cm^{-1} indicating S-S stretching and at 560 cm^{-1} indicating C-S-S-C bonds) increased. Also peaks related to amino acids (tyrosine at 650 cm^{-1} and 848 cm^{-1}, phenylalanine at 1000 cm^{-1}) increased due to hydrolysis of peptides in the media. The peak indicating α-helices increased slightly, furthermore two peaks related to amide III bonds increased tremendously. The increases in protein peaks may result from synthesis of the proteins that are used in the formation of new *S.cerevisiae* cells [72]. Also the strong peak coming from media at 730 cm^{-1} disappeared after 6 hours of incubation for these three spectra, meaning that FAD molecules are internalized into the cells to be used in mitochondria for cellular respiration. When the spectrum of *S.cerevisiae* incubated with 20 ppm m-AgNPs is examined; it can be clearly seen that the same metabolic activities and growth was not observed at this concentration, as the spectrum mostly resembles to the spectrum of its medium.

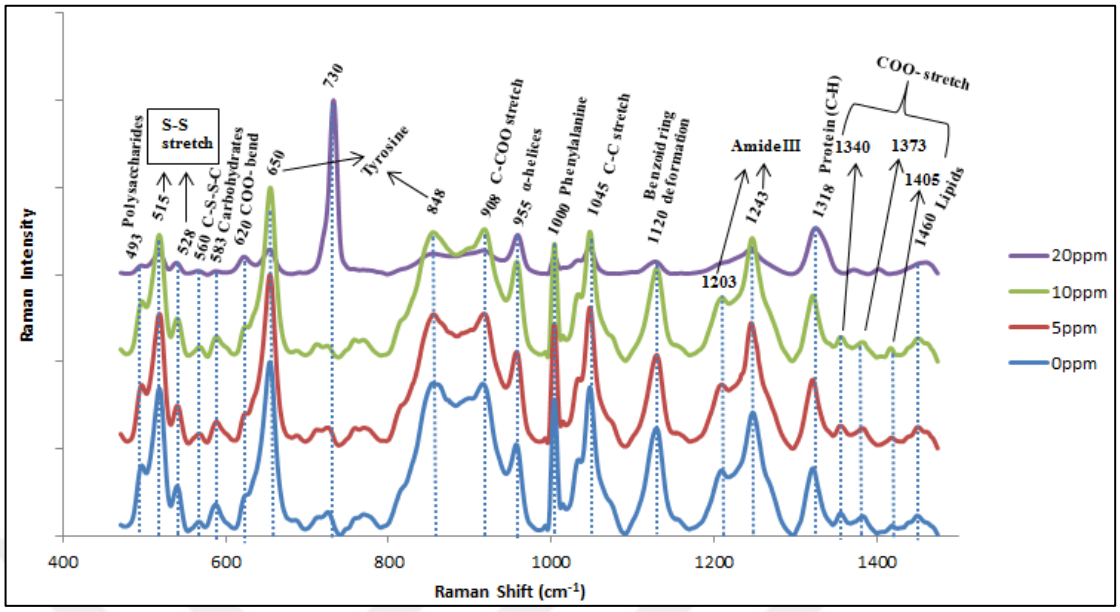

Figure 3.16. The SERS spectra of *S.cerevisiae* after 6 hours of incubation with different concentrations of m-AgNPs

When it comes to 12 hours of incubation, it can be seen that intensities of peaks (for spectra of control, 5 and 10 ppm m-AgNPs) mostly decreased and some of the peaks related with carbohydrates disappeared (493 cm^{-1} and 583 cm^{-1}) according to the SERS spectra in Figure 3.17. The peaks indicating α-helices at 955 cm^{-1}, proteins 1318 cm^{-1} and amide III bond at 1235 cm^{-1} also decreased at 12^{th} hour of cultivation when compared with their SERS spectra at 6 hours of cultivation in Figure 3.16. Peaks related to amino acids (tyrosine and phenylalanine) decreased as they are used as building blocks in metabolic processes. All of these decreases may be observed due to formation of new *S.cerevisiae* cells. Also the intense increase in C-C stretching peak at 1047 cm^{-1} may be coming from chitin structure in the cell wall of yeast [54]. As the number of cells started to increase at 12^{th} hour, an increase is observed in this peak. Also for the spectrum of the control group, a peak at 870 cm^{-1} attributed to C-O-C^{-1}, 4 glycosidic link from carbohydrates can be observed. Intensity of these peaks increased due to the increasing number of cells in the medium.

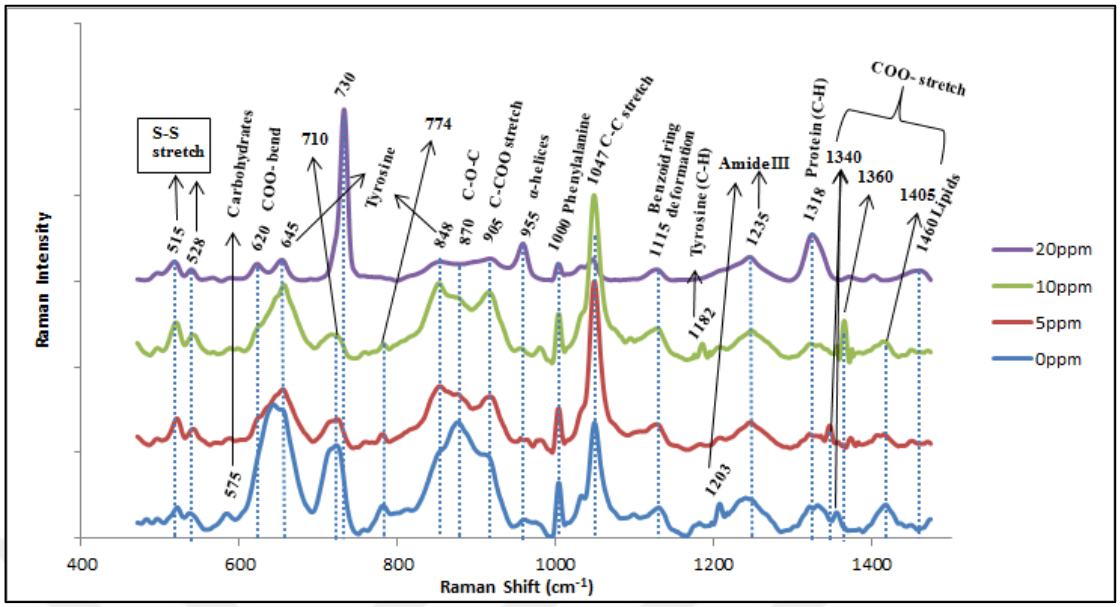

Figure 3.17. The SERS spectra of *S.cerevisiae* after 12 hours of incubation with different concentrations of m-AgNPs

According to Figure 3.18, after 24 hours of incubation, peaks coming from both medium and cells can be seen on the spectra. In the spectra of *S.cerevisiae*/5ppm m-AgNPs and *S.cerevisiae*/10 ppm m-AgNPs, the concentration of metabolites such as amino acids, peptides, nucleic acids and carbohydrates in the medium increased due to metabolic activity. This can be understood both from the increase in the intensities of related peaks; for amino acids (645 cm^{-1}, 850 cm^{-1}, 1170 cm^{-1} and 1000 cm^{-1}), for peptides (1200 cm^{-1}, 1240 cm^{-1} and 1318 cm^{-1}), for carbohydrates (575 cm^{-1} and three peaks in 1327^{-1}-1405 cm^{-1} interval) and from the formation of new bands such as 750 cm^{-1}, 795 cm^{-1} and 1087 cm^{-1}, which are attributed to nucleic acids. If the spectrum of control group is investigated, decreases in intensity was observed for some peaks such as amide III peak at 1240 cm^{-1} and this indicates the end of exponential phase. Small shifts in wavenumber of some peaks result from the change in the chemical content of the environment.

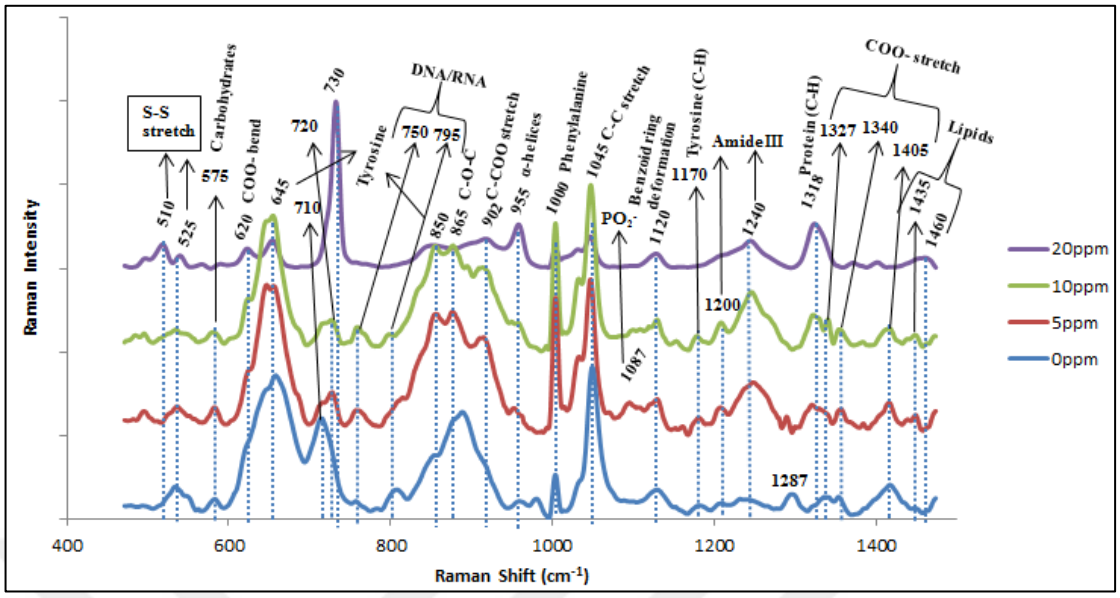

Figure 3.18. The SERS spectra of *S.cerevisiae* after 24 hours of incubation with different concentrations of m-AgNPs

The SERS spectra for *S.cerevisiae* cells that were incubated with different concentrations of m-AgNPs for 48 hours are given in Figure 3.19. When the peaks of culture are investigated after 48 hours of incubation, the intensities of peaks decreased generally, except 1045 cm^{-1} which is probably related with the cell wall structure. The concentration of amino acids in the media decreased compared with 24 hours of incubation but there are still significant amounts of tyrosine and phenylalanine. There is an increase in the intensity of peak at 720 cm^{-1} which can be related to adenine from flavins. The reason for this increase may be the releasing of FAD molecules due to apoptosis or necrosis of the cells [92].

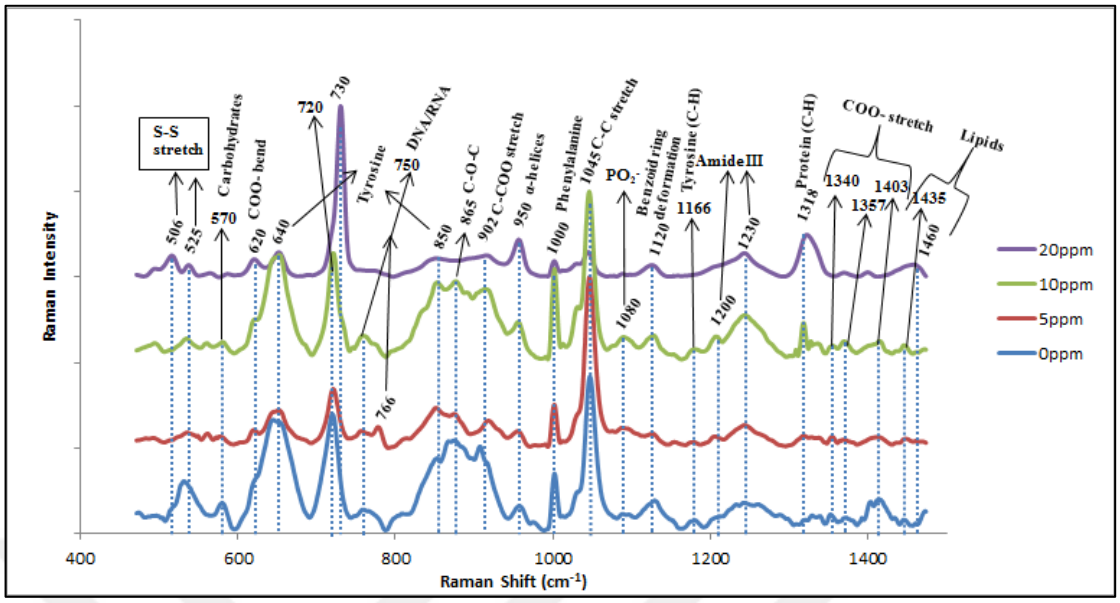

Figure 3.19. The SERS spectra of *S.cerevisiae* after 48 hours of incubation with different concentrations of m-AgNPs

As a result, microbial growth of *S.cerevisiae* did not observed in medium containing 20 ppm m-AgNPs as there is no spectral changes during 48 hours of incubation. On the other hand, concentrations below 20 ppm did not inhibit the growth and metabolic activity of *S.cerevisae* totally, and the SERS spectra similar to the spectrum of control group were obtained. However, the intensities of obtained peaks from *S.cerevisiae*/5ppm m-AgNPs and *S.cerevisiae*/10 ppm m-AgNPs were lower than the peak intensities of control group. This can be seen clearly at the spectra of 12 hours of incubation in Figure 3.17. This result reveals that *S.cerevisiae* cells can grow in size and number in the presence of m-AgNPs at low concentrations such as 5 and 10 ppm but their metabolic activity and number of cells at the end of 48-hour incubation will be lower than control group.

4. CONCLUSIONS

The biocidal effect of AgNPs is a well-known phenomenon. This effect is highly dependent upon the synthesis method and the reducing agents used in synthesis. Smaller size and high dissolution rates of AgNPs increase the effectiveness of nanoparticles as a biocidal agent. When weak reducing agents such as carbohydrates are used in the synthesis of AgNPs, Ag^{+} ions can be released to the medium easily. Although the exact mechanisms are not fully understood, Ag^{0} and Ag^{+} ions both have contribution to biocidal effect of AgNPs. Ag^{0} may interfere with cell wall, nucleic acids or it may inhibit proteins synthesis and metabolic pathways. In the case of Ag^{+} ions, it is believed that they directly affect the replication ability of DNA and inactivate cellular proteins [32]. In this study, AgNPs were reduced by a disaccharide, maltose, and their effect on microbial growth was observed by OD and SERS measurements. Monitoring the media during incubation with m-AgNPs by using SERS, enables to observe chemical changes in the culture media. Bands attributed to vibrations make it possible to detect specific molecules by using the fingerprints of the molecules to be detected.

In this thesis, model microorganisms were selected from two different cell types *E.coli* was used as model organism for bacteria and *S.cerevisiae* was used as model organism for yeast. Three different concentrations of m-AgNPs were tested on each microorganism. The results revealed that when both cells are incubated with 20 ppm m-AgNPs, the proliferation and growth of both microorganisms were inhibited. The other two concentrations of m-AgNPs that are tested were 5 ppm and 10 ppm. According to the changes in the spectral pattern with respect to time, it can be said that formation of certain metabolites were delayed at these concentrations when compared with the spectra of the control group. In the spectra of *E.coli*, it was shown that the intensities of Raman bands attributed to tyrosine, and carbohydrates increased with increasing metabolic activity whereas bands related to proteins (C-H and α-helices) decreased first as the peptones were metabolized then increased due to formation of proteins. The shift in amide III bands, the increase in S-S stretching vibration band and formation of C-N peak after 12 hours of incubation are also related with protein synthesis of *E.coli*. The similar spectral changes in these bands were observed for *E.coli* incubated with 5 ppm and 10 ppm AgNPs and also for the control group. However, spectral changes observed for the control group and *E.coli*

incubated with 5 ppm m-AgNPs can be seen on the spectra of *E.coli* incubated with 10 ppm m-AgNPs at later incubation times. In the case of *S.cerevisiae*, incubation with 5 and 10 ppm m-AgNPs caused decreases in the concentration of metabolites. This is understood by comparing the spectral changes of cell cultures containing these concentrations with the control cell culture. The spectral changes of *S.cerevisiae* were almost the same for the control group, and 5 ppm and 10 ppm m-AgNPs treated cells until 12^{th} hour. Then decreases in the Raman bands related to tyrosine, carbohydrates were observed for cells incubated with 5 and 10 ppm m-AgNPs at the spectra of 12 hours of incubation. This could be result of interaction of m-AgNPs or dissolved Ag+ with DNA/RNA which inhibits the replication process and causes the number of cells in the media remained lower than control group. The intensity of tyrosine, carbohydrates, and amide III bands increased in the spectra of *S.cerevisiae* incubated with 5 and 10 ppm m-AgNPs after 24 hours of incubation, indicating that the growth of cells has taken much more time with respect to the growth at the normal conditions.

In addition to SERS measurements, OD results also show similar patterns which support the SERS results. Depending on the different concentrations of m-AgNPs present in the media, the growth of microorganisms is either suppressed or inhibited. OD results show that the growth is highly affected by the presence of m-AgNPs. The growth of *E.coli* observed in the presence of 5 ppm AgNPs, but the number of cells was lower than control group. When they are incubated with 10 ppm m-AgNPs, the number of cells did not increase much but metabolic activity continued. Lastly, for 20 ppm m-AgNPs OD values decreased with respect to initial value because of biocidal effect of m-AgNPs. When the OD results of *S.cerevisiae* were investigated, it can be said that number of cells of *S.cerevisiae* almost did not increase when the concentration is 20 ppm. The similar results were obtained from the OD graphs of *S.cerevisiae* incubated with 5 ppm and 10 ppm m-AgNPs. Exponential phase of the cells at these concentrations started later than control group.

In conclusion, according to OD and SERS measurements, it can be stated that metabolic activity of both microorganisms are suppressed at lower concentrations of m-AgNPs (5 and 10 ppm m-AgNPs), while metabolic activity and growth is inhibited totally in the presence of 20 ppm m-AgNPs.

5. FUTURE PERSPECTIVES

Biocidal activity of m-AgNPs against model bacteria (*E.coli*) and model yeast (*S.cerevisiae*) cells was demonstrated in this study. The antimicrobial effect has increased with the increasing concentration of m-AgNPs and metabolic activity was monitored by using SERS.

As *S.cerevisae* is widely used in fermentation processes such as making bread, wine, and beer; the fermentation process and possible bacterial contaminations can be monitored by SERS. This method can be applied to industrial microbiological processes. The advantages of SERS can play an important role in the early and fast detection of contamination. The samples can be directly taken from fermentation media and mixed with c-AgNPs. Then the SERS spectra can be obtained rapidly.

The contamination can be prevented with m-AgNPs as they show more severe biocidal effect on bacteria than yeast at 20 ppm concentration. Another study can be the modification of the surface of m-AgNPs in order to increase the cellular uptake of m-AgNPs by bacterial cells. This can enhance the biocidal effect towards bacteria and may increase the chances of eliminating bacterial contamination by using low concentrations of m-AgNPs as antibacterial agent.

REFERENCES

1. Parija SC. *Textbook of microbiology and immunology*. Manesar: Elsevier; 2012.

2. Madigan MT, Martinko JM, Stahl DA, Clark DP. *Brock biology of microorganisms*. San Francisco: Pearson Benjamin-Cummings; 2010.

3. Alberts B, Bray D, Hopkin K, Johnson AD, Lewis J, Raff M, Roberts K, Walter P. *Essential cell biology*. New York: Garland Science, Taylor and Francis Group, LLC; 2015.

4. Berezin S, Aviv Y, Aviv H, Goldberg E, Tischler YR. Replacing a century old technique-modern spectroscopy can supplant gram staining. *Scientific Reports*. 2017;7(1):1–7.

5. Claus D. A standardized gram staining procedure. *World Journal of Microbiology and Biotechnology*. 1992;8(4):451–2.

6. Tille PM. *Bailey and Scott's diagnostic microbiology*. Missouri: Elsevier; 2017.

7. Manolakaki D, Velmahos GC, Kourkoumpetis T, Chang Y, Alam HB, De Moya MM, et al. Candida infection and colonization among trauma patients. *Virulence*. 2010;1(5):367–75.

8. Sayin I, Kahraman M, Sahin F, Yurdakul D, Culha M. Characterization of yeast species using surface-enhanced raman scattering. *Applied Spectroscopy*. 2009;63(11):1276–82.

9. Ene IV, Walker LA, Schiavone M, Lee KK, Martin-Yken H, Dague E, et al. Cell wall remodeling enzymes modulate fungal cell wall elasticity and osmotic stress resistance. *MBio*. 2015;6(4):e00986-15.

10. McKane L, Kandel J. *Microbiology: Essentials and applications.* New York: McGraw-Hill Companies; 1996.

11. Robinson RK. *Encyclopedia of food microbiology*. Oxford: Academic press; 2014.

12. Ingledew WJ, Poole RK. The respiratory chains of escherichia coli. *Microbiological*

Reviews. 1984;48(3):222–71.

13. Rasko DA, Rosovitz MJ, Myers GSA, Mongodin EF, Fricke WF, Gajer P, et al. The pangenome structure of escherichia coli: comparative genomic analysis of e. coli commensal and pathogenic isolates. *Journal of Bacteriology*. 2008;190(20):6881-6893.

14. Moore WR, Anderson ME, Meister A, Murata K, Kimura A. Increased capacity for glutathione synthesis enhances resistance to radiation in escherichia coli: a possible model for mammalian cell protection. *Proceedings of the National Academy of Sciences*. 1989;86(5):1461–1464.

15. Sondi I, Salopek-Sondi B. Silver nanoparticles as antimicrobial agent: a case study on e. coli as a model for gram-negative bacteria. *Journal of Colloid and Interface Science*. 2004;275(1):177–82.

16. Holden PA, Boren D, Ivask A, Godwin HA, Fischer H, Telesca D, et al. Toxicity mechanisms in escherichia coli vary for silver nanoparticles and differ from ionic silver. *Acs Nano*. 2013;8(1):374–86.

17. McQuillan JS, Groenaga Infante H, Stokes E, Shaw AM. Silver nanoparticle enhanced silver ion stress response in escherichia coli K12. *Nanotoxicology*. 2012;6(8):857–66.

18. Zhang L, Jiang Y, Ding Y, Daskalakis N, Jeuken L, Povey M, et al. Mechanistic investigation into antibacterial behaviour of suspensions of ZnO nanoparticles against e. coli. *Journal of Nanoparticle Research*. 2010;12(5):1625-1636.

19. Schwegmann H, Feitz AJ, Frimmel FH. Influence of the zeta potential on the sorption and toxicity of iron oxide nanoparticles on s. cerevisiae and e. coli. *Journal of Colloid and Interface Science*. 2010;347(1):43-48.

20. Baek YW, An YJ. Microbial toxicity of metal oxide nanoparticles (CuO, NiO, ZnO, and Sb_2O_3) to escherichia coli, bacillus subtilis, and streptococcus aureus. *Science of Total Environment*. 2011;409(8):1603-1608.

21. Feldmann H. *Yeast: molecular and cell biology*. Weinheim: John Wiley and Sons; 2011.

22. Cherry JM, Ball C, Weng S, Juvik G, Schmidt R, Adler C, et al. Genetic and physical maps of saccharomyces cerevisiae. *Nature*. 1997;387(6632):67-73.

23. Olivares-Marin IK, González-Hernández JC, Regalado-Gonzalez C, Madrigal-Perez LA. Saccharomyces cerevisiae exponential growth kinetics in batch culture to analyze respiratory and fermentative metabolism. *Journal of Visualized Experiments*. 2018;(139):1–10.

24. Pronk JT, Yde Steensma H, van Dijken JP. Pyruvate metabolism in saccharomyces cerevisiae. *Yeast*. 2002;12(16):1607–33.

25. Bai FW, Anderson WA, Moo-Young M. Ethanol fermentation technologies from sugar and starch feedstocks. *Biotechnology Advances*. 2008;26(1):89–105.

26. Peralta-Yahya PP, Zhang F, Del Cardayre SB, Keasling JD. Microbial engineering for the production of advanced biofuels. *Nature*. 2012;488(7411):320–8.

27. Talebnia F, Karakashev D, Angelidaki I. Production of bioethanol from wheat straw: an overview on pretreatment, hydrolysis and fermentation. *Bioresource Technology*. 2010;101(13):4744–53.

28. Márquez IG, Ghiyasvand M, Massarsky A, Babu M, Samanfar B, Omidi K, et al. Zinc oxide and silver nanoparticles toxicity in the baker's yeast, saccharomyces cerevisiae. *PLoS One*. 2018;13(3):1–20.

29. Dorobantu LS, Fallone C, Noble AJ, Veinot J, Ma G, Goss GG, et al. Toxicity of silver nanoparticles against bacteria, yeast, and algae. *Journal of Nanoparticle Research*. 2015;17(4):172.

30. Suppi S, Kasemets K, Ivask A, Künnis-Beres K, Sihtmäe M, Kurvet I, et al. A novel method for comparison of biocidal properties of nanomaterials to bacteria, yeasts and algae. *Journal of Hazardous Materials*. 2015;286(6):75–84.

31. Park S, Park HH, Kim SY, Kim SJ, Woo K, Ko G. Antiviral properties of silver nanoparticles on a magnetic hybrid colloid. *Applied and Environmental Microbiology*. 2014;80(8):2343–50.

32. Guzman M, Dille J, Godet S. Synthesis and antibacterial activity of silver

nanoparticles against gram-positive and gram-negative bacteria. *Nanomedicine: Nanotechnology, Biology and Medicine*. 2012;8(1):37–45.

33. Kheybari S, Samadi N, Hosseini SV, Fazeli A, Fazeli MR. Synthesis and antimicrobial effects of silver nanoparticles produced by chemical reduction method. *DARU Journal of Pharmaceutical Sciences*. 2010;18(3):168–72.

34. Yang HW, Hua MY, Liu HL, Huang CY, Wei KC. Potential of magnetic nanoparticles for targeted drug delivery. *Nanotechnology, science and applications*. 2012;5(1):73-86.

35. Mohanraj VJ, Barnes TJ, Prestidge CA. Silica nanoparticle coated liposomes: a new type of hybrid nanocapsule for proteins. *International Journal of Pharmaceutics*. 2010;392(1–2):285–93.

36. Wang C, Yu C. Analytical characterization using surface-enhanced raman scattering (sers) and microfluidic sampling. *Nanotechnology*. 2015;26(9):92001.

37. Zhang L, Gong X, Bao Y, Zhao Y, Xi M, Jiang C, et al. Electrospun nanofibrous membranes surface-decorated with silver nanoparticles as flexible and active/sensitive substrates for surface-enhanced raman scattering. *Langmuir*. 2012;28(40):14433–40.

38. Jung JH, Oh HC, Noh HS, Ji JH, Kim SS. Metal nanoparticle generation using a small ceramic heater with a local heating area. *Journal of Aerosol Science*. 2006;37(12):1662–70.

39. Tseng KH, Lee HL, Tien DC, Tang YL, Kao YS. A Study of antibioactivity of nanosilver colloid and silver ion solution. *Advances in Materials Science and Engineering*. 2014;2014(1):1–6.

40. Suresh AK, Pelletier DA, Wang W, Moon J-W, Gu B, Mortensen NP, et al. Silver nanocrystallites: biofabrication using shewanella oneidensis, and an evaluation of their comparative toxicity on gram-negative and gram-positive bacteria. *Environmental Science and Technology*. 2010;44(13):5210–5.

41. Panáček A, Kvitek L, Prucek R, Kolář M, Večeřová R, Pizúrová N, Zbořil R, et al. Silver colloid nanoparticles: synthesis, characterization, and their antibacterial

activity. *The Journal of Physical Chemistry B*. 2006;110(33):16248-16253.

42. Çulha M, Kalay Ş, Sevim E, Pinarbaş M, Baş Y, Akpinar R, et al. Biocidal properties of maltose reduced silver nanoparticles against american foulbrood diseases pathogens. *Biometals*. 2017;30(6):893–902.

43. Kahraman M, Keseroğlu K, Çulha M. On sample preparation for surface-enhanced raman scattering (sers) of bacteria and the source of spectral features of the spectra. *Applied Spectroscopy*. 2011;65(5):500–6.

44. Ferraro JR, Nakamoto K. *Introductory Raman Spectroscopy*. San Diego: Elsevier; 2003.

45. Atkins PW, Overton T. *Shriver and Atkin's inorganic chemistry*. Oxford: Oxford University Press; 2010.

46. Raman CV, Krishnan KS. A new type of secondary radiation. *Nature*. 1928;121(3048):501.

47. Zedler L, Hager MD, Schubert US, Harrington MJ, Schmitt M, Popp J, et al. Monitoring the chemistry of self-healing by vibrational spectroscopy - current state and perspectives. *Materials Today*. 2014;17(2):57–69.

48. Bumbrah GS, Sharma RM. Raman spectroscopy – basic principle, instrumentation and selected applications for the characterization of drugs of abuse. *Egyptian Journal of Forensic Sciences*. 2016;6(3):209–15.

49. Cam D, Keseroglu K, Kahraman M, Sahin F, Culha M. Multiplex identification of bacteria in bacterial mixtures with surface-enhanced raman scattering. *Journal of Raman Spectroscopy*. 2010;41(5):484–9.

50. Kahraman M, Karatas OF, Aydin O, et al. Nanoplasmonics in biosensing and nanobiomedicine. *Encyclopedia of Nanoscience and Nanotechnology*. 2011:289–305.

51. Sevenler D, Ünlü NL, Ünlü MS. Nanoparticle biosensing with interferometric reflectance imaging. *Nanobiosensors and Nanobioanalyses*. 2015:81-95.

52. Mikac L, Ivanda M, Gotić M, Mihelj T, Horvat L. Synthesis and characterization of

silver colloidal nanoparticles with different coatings for sers application. *Journal of Nanoparticle Research*. 2014;16(12):2748.

53. Meng W, Hu F, Jiang X, Lu L. Preparation of silver colloids with improved uniformity and stable surface-enhanced raman scattering. *Nanoscale Research Letters*. 2015;10(1):1–8.

54. Sujith A, Itoh T, Abe H, Yoshida KI, Kiran MS, Biju V, et al. Imaging the cell wall of living single yeast cells using surface-enhanced raman spectroscopy. *Analytical and Bioanalytical Chemistry*. 2009;394(7):1803–9.

55. Zhou H, Yang D, Ivleva NP, Mircescu NE, Niessner R, Haisch C. Sers detection of bacteria in water by in situ coating with Ag nanoparticles. *Analytical Chemistry*. 2014;86(3):1525–33.

56. Lemma T, Wang J, Arstila K, Hytönen VP, Toppari JJ. Identifying yeasts using surface enhanced raman spectroscopy. *Spectrochimica Acta Part A: Molecular and Biomolecular Spectroscopy*. 2019;218(13):299–307.

57. Culha M, Kahraman M, Çam D, Sayin I, Keseroğlu K. Rapid identification of bacteria and yeast using surface-enhanced raman scattering. *Surface and Interface Analysis*. 2010;42(6–7):462–5.

58. Chao Y, Zhang T. Surface-enhanced raman scattering (sers) revealing chemical variation during biofilm formation: from initial attachment to mature biofilm. *Analytical and Bioanalytical Chemistry*. 2012;404(5):1465–75.

59. Efeoglu E, Culha M. In situ – monitoring of biofilm formation by using surface-enhanced raman scattering. *Applied Spectroscopy.* 2013;67(5):498–505.

60. Efeoglu E, Culha M. Surface-enhanced raman scattering for biofilm characterization. *Spectroscopy.* 2013;28(11):36-41.

61. Keleştemur S, Çulha M. Understanding and discrimination of biofilms of clinically relevant microorganisms using surface-enhanced raman scattering. *Applied Spectroscopy.* 2017;71(6):1180-8.

62. Premasiri WR, Lee JC, Sauer-Budge A, Théberge R, Costello CE, Ziegler LD. The

biochemical origins of the surface-enhanced raman spectra of bacteria : a metabolomics profiling by sers. *Analytical and Bioanalytical Chemistry*. 2016;408(17):4631-47.

63. Kahraman M, Sur I, Culha M. Label-free detection of proteins from structures using surface-enhanced raman scattering. *Analytical Chemistry*. 2010;82(18):7596–602.

64. Shanmukh S, Jones L, Driskell J, Zhao Y, Dluhy R, Tripp RA. Rapid and sensitive detection of respiratory virus molecular signatures using a silver nanorod array sers substrate. *Nano Letters*. 2006;6(11):2630–6.

65. Yang Y, Zhang Z, He Y, Wang Z, Zhao Y, Sun L. Fabrication of Ag@TiO_2 electrospinning nanofibrous felts as sers substrate for direct and sensitive bacterial detection. *Sensors and Actuators B: Chemical*. 2018;273(20):600–9.

66. Grubisha DS, Lipert RJ, Park H-Y, Driskell J, Porter MD. Femtomolar detection of prostate-specific antigen: an immunoassay based on surface-enhanced raman scattering and immunogold labels. *Analytical Chemistry*. 2003;75(21):5936–43.

67. Mohs AM, Mancini MC, Singhal S, Provenzale JM, Leyland-Jones B, Wang MD, et al. Hand-held spectroscopic device for in vivo and intraoperative tumor detection: contrast enhancement, detection sensitivity, and tissue penetration. *Analytical Chemistry*. 2010;82(21):9058–65.

68. An JH, El-Said WA, Yea CH, Kim TH, Choi W. Surface-enhanced raman scattering of dopamine on self-assembled gold nanoparticles. *Journal of Nanoscience and Nanotechnology*. 2011;11(5):4424-4429.

69. Myers FB, Lee LP. Innovations in optical microfluidic technologies for point-of-care diagnostics. *Lab on a Chip*. 2008;8(12):2015–31.

70. Notingher I. Raman spectroscopy cell-based biosensors. *Sensors*. 2007;7(8):1343–58.

71. Chrimes AF, Khoshmanesh K, Stoddart PR, Mitchell A, Kalantar-Zadeh K. Microfluidics and raman microscopy: current applications and future challenges. *Chemical Society Reviews*. 2013;42(13):5880–906.

72. Singh GP, Volpe G, Creely CM, Grötsch H, Geli IM, Petrov D. The lag phase and G1 phase of a single yeast cell monitored by raman microspectroscopy. *Journal of Raman Spectroscopy*. 2006;37(8):858–64.

73. Iversen JA, Berg RW, Ahring BK. Quantitative monitoring of yeast fermentation using raman spectroscopy. *Analytical and Bioanalytical Chemistry*. 2014;406(20):4911–9.

74. Lee PC, Meisel D. Adsorption and surface-enhanced raman of dyes on silver and gold sols. *The Journal of Physical Chemistry*. 1982;86(17):3391–5.

75. Pillai ZS, Kamat P V. What factors control the size and shape of silver nanoparticles in the citrate ion reduction method? *The Journal of Physical Chemistry B*. 2004;108(3):945–51.

76. Horiba Raman data and analysis: Jobin Yvon Inc 2007 [cited 2019 28 May]. Available from: http://www.horiba.com/fileadmin/uploads/Scientific/Documents/Raman/bands.pdf

77. Çulha M, Adigüzel A, Yazici MM, Kahraman M, Şahin F, Güllüce M. Characterization of thermophilic bacteria using surface-enhanced raman scattering. *Applied Spectroscopy*. 2008;62(11):1226–32.

78. Maquelin K, Kirschner C, Choo-Smith LP, Van Den Braak N, Endtz HP, Naumann D, et al. Identification of medically relevant microorganisms by vibrational spectroscopy. *Journal of Microbiological Methods*. 2002;51(3):255-271.

79. Premasiri WR, Moir DT, Klempner MS, Krieger N, Jones G, Ziegler LD. Characterization of the surface enhanced raman scattering (sers) of bacteria. *The Journal of Physical Chemistry B*. 2005;109(1):312-320.

80. Jarvis RM, Goodacre R. Characterisation and identification of bacteria using sers. *Chemical Society Reviews*. 2008;37(5):931-936.

81. Schkolnik G, Schmidt M, Mazza MG, Harnisch F, Musat N. In situ analysis of a silver nanoparticle-precipitating shewanella biofilm by surface enhanced confocal raman microscopy. *PLoS One*. 2015;10(12):e0145871.

82. Carey PR, Gibson BR, Gibson JF, Greenberg ME, Heidari-Torkabadi H, Pusztai-Carey M, et al. Defining molecular details of the chemistry of biofilm formation by raman microspectroscopy. *Biochemistry*. 2017;56(17):2247-2250.

83. Horiba Raman Spectroscopy for proteins application scientist: Jobin Yvon Inc 2007 [cited 2019 28 May] Available from: http://www.horiba.com/fileadmin/uploads/Scientific/Documents/Raman/HORIBA_webinar_proteins.pdf

84. Naumann D. Infrared and nir raman spectroscopy in medical microbiology. *Infrared spectroscopy: new tool in medicine, BiOS '98 International Biomedical Optics Symposium*; 1998: International Society for Optis and Photonics.

85. Jarvis RM, Law N, Shadi IT, O'Brien P, Lloyd JR, Goodacre R. Surface-enhanced raman scattering from intracellular and extracellular bacterial locations. *Analytical Chemistry*. 2008;80(17):6741-6746.

86. Ivleva NP, Wagner M, Horn H, Niessner R, Haisch C. In situ surface-enhanced raman scattering analysis of biofilm. *Analytical Chemistry*. 2008;80(22):8538-44.

87. Krafft C, Neudert L, Simat T, Salzer R. Near infrared raman spectra of human brain lipids. *Spectrochimica Acta Part A: Molecular and Biomolecular Spectroscopy*. 2005;61(7):1529-1535.

88. Stone N, Kendall C, Smith J, Crow P, Barr H. Raman spectroscopy for identification of epithelial cancers. *Faraday Discussions*. 2004;126(2):141-157.

89. Hud N V., Balhorn R, Milanovich FP. Evidence of novel secondary structure in DNA-bound protamine is revealed by raman spectroscopy. *Biochemistry*. 1994;33(24):7528-7535.

90. Park C, Lee YJ, Yup Lee S, Bin Oh H, Lee J. Determination of the intracellular concentrations of metabolites in escherichia coli collected during the exponential and stationary growth phases using liquid chromatography-mass spectrometry. *Bulletin of the Korean Chemical Society*. 2011;32(2):524-530.

91. Vollmer W, Blanot D, De Pedro MA. Peptidoglycan structure and architecture. *FEMS Microbiology Reviews*. 2008;32(2):149–67.

92. Kiran MS, Itoh T, Abe H, Fujita Y, Tomimoto K, Biju V, et al. Sers microscopic imaging as novel tool for assessing viability and enumerating yeast cells at various stages of cell cycle in lag, log, exponential and stationary phases of growth in culture. *Journal of Experimental Nanoscience*. 2014;9(10):1003–14.